AGU PUBLICATIONS

JGR

Journal of Geophysical Research: Oceans

RESEARCH ARTICLE

10.1002/2014JC009901

Mean sea level variability in the North Sea: Processes and implications

Sönke Dangendorf[1], Francisco M. Calafat[2], Arne Arns[1], Thomas Wahl[3,4], Ivan D. Haigh[5], and Jürgen Jensen[1]

[1]Research Institute for Water and Environment, University of Siegen, Siegen, Germany, [2]National Oceanography Centre, Southampton, UK, [3]College of Marine Science, University of South Florida, St. Petersburg, Florida, USA, [4]Research Centre Siegen, University of Siegen, Siegen, Germany, [5]Ocean and Earth Science, University of Southampton, National Oceanography Centre, Southampton, UK

Key Points:
- North Sea mean sea level variability over the past 140 years is analyzed
- The variability is mainly related to local and remote atmospheric forcing
- The variability hampers early detection of sea level rise acceleration

Correspondence to:
S. Dangendorf,
soenke.dangendorf@uni-siegen.de

Citation:
Dangendorf, S., F. M. Calafat, A. Arns, T. Wahl, I. D. Haigh, and J. Jensen (2014), Mean sea level variability in the North Sea: Processes and implications, *J. Geophys. Res. Oceans*, *119*, 6820–6841, doi:10.1002/2014JC009901.

Received 11 FEB 2014
Accepted 16 SEP 2014
Accepted article online 19 SEP 2014
Published online 15 OCT 2014

Abstract Mean sea level (MSL) variations across a range of time scales are examined for the North Sea under the consideration of different forcing factors since the late 19th century. We use multiple linear regression models, which are validated for the second half of the 20th century against the output of a tide-surge model, to determine the barotropic response of the ocean to fluctuations in atmospheric forcing. We find that local atmospheric forcing mainly initiates MSL variability on time scales up to a few years, with the inverted barometric effect dominating the variability along the UK and Norwegian coastlines and wind controlling the MSL variability in the south from Belgium up to Denmark. On decadal time scales, MSL variability mainly reflects steric changes, which are largely forced remotely. A spatial correlation analysis of altimetry observations and gridded steric heights suggests evidence for a coherent signal extending from the Norwegian shelf down to the Canary Islands. This fits with the theory of longshore wind forcing along the eastern boundary of the North Atlantic causing coastally trapped waves to propagate over thousands of kilometers along the continental slope. Implications of these findings are assessed with statistical Monte-Carlo experiments. It is demonstrated that the removal of known variability increases the signal to noise ratio with the result that: (i) linear trends can be estimated more accurately; (ii) possible accelerations (as expected, e.g., due to anthropogenic climate change) can be detected much earlier. Such information is of crucial importance for anticipatory coastal management, engineering, and planning.

1. Introduction

Sea level rise (SLR) is one of the most certain consequences of climate change. Due to this and its broad socioeconomic and environmental impact on coastal zones, SLR has become a topic of major importance for scientists, governments, and the general public. Hence, significant efforts have been devoted to better understand the processes driving SLR and variability with the aim of producing more accurate projections of future SLR, which can then serve as the basis for implementing appropriate adaptation measures. The challenge is to protect coastal zones against the impacts of SLR and assure high safety standards not only under present day but also future climate conditions. This complex task requires an extensive understanding of how sea level has changed in the past and might change in the future, on both regional and global scales.

There is observational evidence that global mean sea level (MSL; interpreted in terms of the volume of the global ocean) has risen at a mean rate of about 1.7 mm/yr during the 20th century [*Church et al*., 2013], and scientific consensus is that it will continue to rise through the 21st century: most likely at an accelerated rate, due to enhanced greenhouse gas emissions [e.g., *Meehl et al*., 2007; *Vermeer and Rahmstorf*, 2009; *Church et al*., 2013; *Orlic and Pasaric*, 2013]. Furthermore, it has been known for some time that the rate of SLR is not uniform but varies widely by region and over time, with some regions experiencing a much larger (or smaller) SLR than the global average [e.g., *Douglas*, 1991; *Church et al*., 2013]. Additionally, some regions experience vertical land movements (VLM), which can further increase/decrease the risk of rising sea levels.

Some authors have claimed that the global MSL budget (interpreted in terms of the volume of the global ocean) can be reasonably closed within the observational errors by finding that the sum of its two major

components (i.e., the mass and steric) agrees well with observations of total MSL for the past 50 years [*Church et al*., 2011]. However, accurate local and regional budget analyses are still rare. The difficulty is related to the dynamic character of each component producing its individual regional pattern [*Mitrovica et al*., 2001; *Levermann et al*., 2005; *Yin et al*., 2009; *Riva et al*., 2010; *Slangen et al*., 2011]. Additionally, each component is further characterized by its own temporal variability acting on time scales ranging from months to several decades [e.g., *Sturges and Douglas*, 2011; *Calafat et al*., 2012, 2013; *Calafat and Chambers*, 2013]. Hence, understanding the regional dynamics of SLR and variability requires a careful assessment of each component separately before exploring the combined regional budget.

In this paper, we investigate the mechanisms of intra-annual to decadal-scale MSL variability as measured by tide gauges (often referred to as local or relative sea level) in the North Sea basin with a particular focus on local and remote atmospheric forcing. Recently, an assessment of North Sea MSL changes from the early 19th century onward was undertaken by *Wahl et al*. [2013]. The authors focused on long-term changes in terms of geocentric (sometimes referred to as "absolute") and relative MSL changes based on annually averaged time series. The study revealed that geocentric MSL rose by 1.6 mm/yr since 1900, a rate which is close to that of the global mean rate over the 20th century [*Church and White*, 2011]. The authors found acceleration in geocentric MSL around the end of the 19th century, prior to which geocentric MSL was relatively stable in the North Sea. Over the last few decades, an additional acceleration was found, but it was concluded that the recent high rates of SLR over the period were not unusual compared to the high rates observed at the end of the 19th century. In terms of variability, only fluctuations in the mean local sea level pressure (SLP) were compared to the MSL and it was found that, although they explain a significant fraction of the interannual variability in sea level, they fail to explain the major multidecadal features.

Here we extend the study of *Wahl et al*. [2013] by assessing the characteristics of intra-annual to decadal-scale variability in more detail in order to better understand the processes driving the observed sea level changes from the late 19th century onward. Improving our understanding of such processes is essential to produce better regional projections of potential future sea level rise, and thus contribute to more effective coastal planning. In a recent paper, *Haigh et al*. [2014] highlighted that the presence of significant interannual to decadal variations linked to internal climate variability hampers the early detection of sea level accelerations linked to anthropogenic climate change and showed that removal of such variability will reduce the detection time. While reducing the noise is important, a careful assessment of processes contributing to SLR and variability is crucial to assess whether recent or possible future accelerations in sea level represent a temporal fluctuation relating to internal climate variability or are the response to anthropogenic forcing. From an engineering perspective, it is further important to understand the sources of variability as elevated sea levels enhance the risk of coastal flooding.

Investigations of local MSL variability in the North Sea on intra and interannual time scales have already been conducted by various authors [e.g., *Plag and Tsimplis*, 1999; *Yan et al*., 2004; *Wakelin et al*., 2003; *Tsimplis et al*., 2005; *Jevrejeva et al*., 2005; *Albrecht and Weisse*, 2012; *Dangendorf et al*., 2012, 2013a, 2013b; *Richter et al*., 2012]. *Plag and Tsimplis* [1999] assessed the (nonstationary) seasonal cycle of MSL and found that, in the North Sea region, it is considerably affected by atmospherically induced variability. *Yan et al*. [2004] reported a strong link between local MSL variability and the North Atlantic Oscillation (NAO), a major mode of large-scale atmospheric variability in the North Atlantic region [*Hurrell*, 1995]. This link is mainly related to the response of sea level to well-understood wind and pressure forcing [*Wakelin et al*., 2003; *Albrecht and Weisse*, 2012; *Dangendorf et al*., 2012; *Richter et al*., 2012] and to changes in the position and intensity of the NAO's centers of action [*Kolker and Hameed*, 2007]. However, the aforementioned studies are either based on numerical modeling studies limited to the second half of the 20th century and/or focused on specific seasons and coastline stretches [e.g., *Richter et al*., 2012; *Dangendorf et al*., 2013a]. The role of atmospheric forcing on longer time scales and its contribution to acceleration/deceleration patterns in the entire region has not been explored. Furthermore, none of the above mentioned studies investigated the nature of decadal variations, which are present in the records [*Dangendorf et al*., 2013a, 2013b; *Woodworth et al*., 2009]. *Sturges and Douglas* [2011] and *Calafat et al*. [2012] found that a significant fraction of the decadal-scale MSL variability along the eastern boundary of the North Atlantic can be explained as a response to changes in longshore winds, including the generation and propagation of coastally trapped waves. They also showed that such variability is part of a large coherent signal extending thousands of kilometers along the European Atlantic coast from the Canary Islands up to the coast of Ireland. *Calafat et al*. [2013] furthermore

showed that this coherent signal also propagates into large parts of the Nordic Seas and even into parts of the Arctic Ocean, while *Marcos et al*. [2013] demonstrated a similar response to the longshore wind in the tropical Atlantic at the Tenerife tide gauge. Whether this signal affects the North Sea, and if so, by how much, is a question yet to be answered.

Here we examine the nature of intra-annual to decadal-scale MSL variability observed from a set of 22 long tide gauge records from the North Sea basin for the 140 year period from 1871 to 2011. This is done by consecutively investigating the variability in different frequency bands and exploring possible driving mechanisms. We start by assessing the temporal and spatial characteristic of high frequency variability in the basin before extending the study area to the Northeast Atlantic in order to examine its influence on the North Sea. To integrate spatial information into the analysis, we use gridded satellite altimetry measurements and gridded temperature data. Plausible mechanisms are explored by combining atmospheric and oceanographic measurements, either local or remote, which are then used to reconstruct decadal-scale fluctuations in the North Sea basin. Following that, we use statistical experiments to test whether the removal of known parts of the variability influences the: (i) robustness of linear trend estimations and (ii) the interpretation of acceleration and deceleration patterns as expected under different future greenhouse gas emission scenarios.

The paper is structured as follows. The data and methods used are described in section 2. Results are presented and discussed in section 3, and conclusions are given in section 4.

2. Data and Methods

2.1. Data

A set of North Sea tide gauge records, similar to that used by *Wahl et al*. [2013] for the investigation of the inner North Sea, is examined. The region is shown in Figure 1a and spans from the eastern boundary of the English Channel along the southern coastlines and the Norwegian Trench to the eastern coastline of the UK. In contrast to *Wahl et al*. [2013], the records from the English Channel are not included in our analysis. A total of 22 tide gauge records at monthly resolution were selected, 18 of which were downloaded from the webpage of the Permanent Service for Mean Sea Level (PSMSL) [*Holgate et al*., 2013], while the other four (from the German Bight) were reconstructed by *Wahl et al*. [2010, 2011]. The records span different periods with some of them starting in the early 19th century. Since we are interested in the link between atmospheric forcing and MSL variability, only the period for which both atmospheric and MSL data are available (i.e., from 1871 to 2011, see also below) is analyzed.

In addition to the individual stations, we compute and analyze five MSL index time series, representing the mean of four subregions (region 1, southwestern North Sea: stations 1–6; region 2, southeastern North Sea: stations 7–14; region 3, northeastern North Sea: stations 15–17; region 4, northwestern North Sea: stations 18–22) and the mean of all stations (North Sea). The indices are calculated following the method used by *Haigh et al*. [2009] and *Wahl et al*. [2011], which consists of differentiating the time series at each station (thereby removing the linear trend), averaging the residuals across stations, and then adding the averaged residuals cumulatively. The mean seasonal cycle (determined by the long-term average of each month) is removed from all time series prior to the analyses. Decadal-scale features are examined by applying a 48 month moving average filter to the deseasonalized monthly records.

While the tide gauge records give unique insights into temporal variability of coastal sea level on long time scales, spatial dependencies between the open ocean and the coastal sea level are—due to the lack of information—much harder to assess. Therefore, we complement our data set with satellite altimetry data for the northeast Atlantic. Although the records are limited in time, they provide near-global coverage making them a valuable source for the investigation of spatial characteristics. Here we use monthly averaged sea surface height (SSH) anomalies (corrected for the inverse barometer effect (IBE)) from TOPEX/Poseidon, ERS-1/2, and Envisat on a $1/3^\circ \times 1/3^\circ$ Mercartor grid spanning the period from January 1993 to December 2011 and obtained from AVISO [*Ducet and Le Traon*, 2001]. The processing carried out on the altimetry data set (i.e., the removal of the seasonal cycle and the smoothing) is identical to that undertaken for the tide gauge records.

We also analyze the output from a barotropic version (Tide+Surge Model, hereafter TSM) of the Hamburg Shelf Ocean Model (HAMSOM [*Chen*, 2014]). The TSM data are used to investigate the performance of the

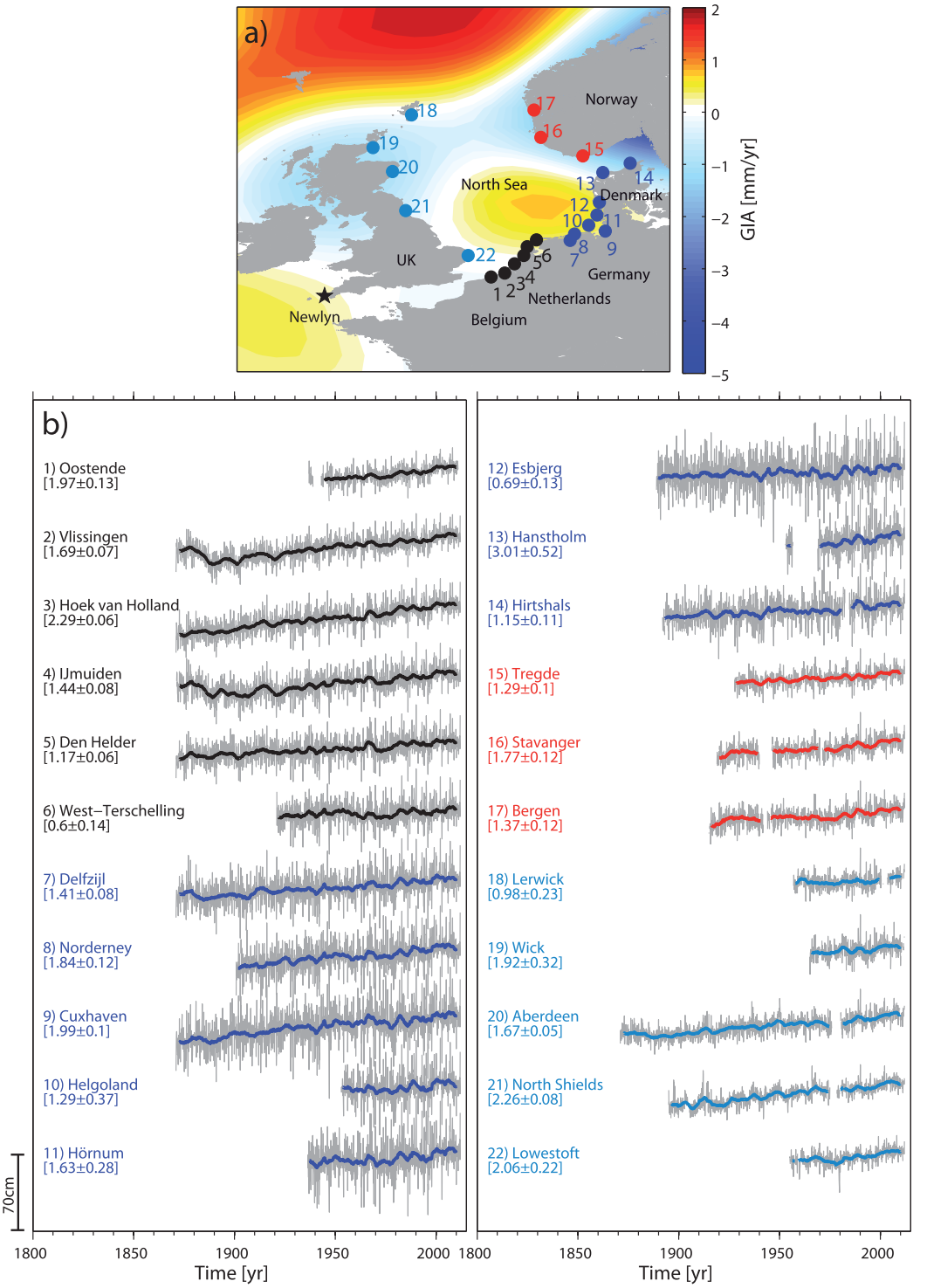

Figure 1. (a) Investigation area and tide gauge locations with their station IDs. The GIA contribution as provided by *Peltier* [2004] is also shown. (b) Monthly deseasonalized local MSL (gray), where the GIA contribution is already removed, and a 48 month low-pass filtered version (black) for each tide gauge considered in the present study. Each station name together with its ID is shown beside the time series. The linear trend with its 2σ SE for the full available period at each location is also given. The colors in Figures 1a and 1b refer to the four subregions defined in the text.

statistical-empirical linear regression models (LRMs) described in section 2.2 below. The model was run for the period 1953–2003. The TSM has a horizontal and temporal resolution of 3 km and 5 min, respectively. It covers the entire North Sea region bounded by the Shetland Islands in the north, the Dover Strait in the

south, the Orkney Islands in the west, and the Baltic Sea in the east. The TSM is nested into a larger Northwest European Shelf model (NWESM) also based on HAMSOM, extending over the region from 47°N to 63°N and 15°W to 14°E. The NWESM is forced by the main tidal constituents at the model boundaries as well as gridded surface wind and pressure data from the NCEP/NCAR reanalysis [*Kalnay et al*., 1996]. More information on the model is provided by *Chen* [2014].

To examine the contribution of atmospheric forcing, gridded data sets from the 20th century reanalysis project (20CRv2) are evaluated. The 20CRv2 data represent the output of a global weather forecast model that assimilates six-hourly SLP observations, monthly sea surface temperature (SST), and sea ice extent observations [*Compo et al*., 2011]. Time series of monthly mean SLP and zonal and meridional wind stress from the 20CRv2 are available on a $2^\circ \times 2^\circ$ global grid and were downloaded from the webpage (http://www.esrl.noaa.gov/psd/data/20thC_Rean/) of the National Oceanic and Atmospheric Administration (NOAA). The time series of SLP and wind stress are processed similarly to the tide gauge records, that is, the mean seasonal cycle is removed; for decadal-scale investigations, the time series are then smoothed with a 48 month moving average filter. Note that before 1900, the 20CRv2 data have been found to be affected by model internal inconsistencies [*Dangendorf et al*., 2014], which are probably related to the lack of data available for assimilation in the early periods [*Krueger et al*., 2013], and thus results for this period should be interpreted with caution. Nevertheless, these inconsistencies were found to affect mostly extreme values whereas their impact on monthly means is suggested to be much smaller [*Dangendorf et al*., 2014].

Since the HAMSOM TSM run is forced by NCEP/NCAR reanalysis wind and SLP fields [*Kalnay et al*., 1996], we also use wind stress and SLP fields from the NCEP/NCAR reanalysis (available from the NOAA webpage) to further validate the LRMs. Unlike the 20CRv2, the NCEP/NCAR reanalysis only covers the period from 1948 to present. This is sufficient for our purposes since we use the data to validate the LRMs by comparing their outputs with those of the TSM for the period from 1952 to 2003.

For the assessment of steric MSL changes (see the Methods section for details on their calculation), the global gridded temperature and salinity data set by *Ishii and Kimoto* [2009] is used. This data consist of monthly $1^\circ \times 1^\circ$ gridded fields covering the upper 1500 m of the water column with 24 unevenly distributed vertical levels and spanning the period 1945–2011. In addition to the gridded temperature and salinity fields, we examine in situ measurements from a hydrographic station. Because of the special characteristics of the shallow shelf in the North Sea (with water depths mostly less than 100 m), we restrict the examination of hydrographic data to the station of Sognesjoen. The station is located in the Norwegian Trench and provides temperature and salinity profiles covering the whole water column down to 300 m from 1950 to 2011 (http://www.imr.no/forskning/forskningsdata/stasjoner/).

2.2. Methods

The main focus of our study is on temporal variations of MSL as measured by tide gauges in the North Sea and their physical and geographical origin. It is important to note that tide gauges measure sea level relative to a benchmark on land (often referred to as local or relative sea level) or equivalently variations in the local distance from the sea surface to the seafloor. Local MSL variations can be viewed as the sum of three contributions: (1) changes in ocean bottom pressure (OBP), (2) changes in SLP, and (3) density changes due to temperature and salinity variations (the resulting sea level changes are often referred to as steric changes). Using this separation, local MSL changes can be described by:

$$\eta_{local} = \eta_{OBP} + \eta_{SLP} + \eta_{steric} \tag{1}$$

The first term, η_{OBP}, accounts for OBP changes resulting from both VLMs and any mass transport in the Earth system, including the effect of such mass transport on the gravity field as well as water mass transport and redistribution in the ocean induced by changes in atmospheric forcing. Note that, although changes in SLP cause water mass redistribution, they are not accompanied by OBP changes (departures from classical IB effect are usually small outside the tropics [*Wunsch and Stammer*, 1997]), and thus they are included in a different term (η_{SLP}). In general, the contribution of η_{OBP} can be directly measured by OBP recorders or satellite gravimetry. However, OBP recorders are absent in the region, and gravimetry observations do not have sufficient spatial (and temporal) resolution for local studies. Hence, in practice, direct observations of η_{OBP} are not available in the region. The contribution of the SLP term, η_{SLP}, can be directly calculated by using SLP

data and assuming that variations in SLP cause local MSL to change at a rate of −1 cm/hPa, which is, in essence, the inverse barometer approximation.

The steric term, η_{steric}, can also be computed directly by vertically integrating the density anomalies (derived from the temperature and salinity data) at each grid point and for each time step, using the following equation:

$$\eta_{steric} = -\frac{1}{\rho_0}\int_{-H}^{0}(\rho-\bar{\rho})dz \tag{2}$$

where ρ_0 is a reference density (1025 kg/m^3), H is the reference depth, ρ is the in situ density of sea water (calculated using the nonlinear equation of state for seawater), z denotes depth, and the overbar indicates time average taken over the entire investigation period from 1945 to 2011. Because temperature and salinity observations are usually scarce below 700 m, we reference the steric height to two different levels: 200 and 700 m. The steric height is deseasonalized prior to the analysis of the local MSL.

As mentioned previously, VLMs are reflected on OBP changes. VLMs generally stem from two different mechanisms: glacial isostatic adjustment (GIA), which is associated with the Earth's viscoelastic response to the last deglaciation, and tectonic effects coupled with local processes such as groundwater withdrawal, and earth quakes, or regional effects resulting from changes in land ice cover [e.g., *Jiang et al*., 2010] or changes in land water storage [e.g., *Amos et al*., 2014]. The contribution of VLMs to η_{OBP} can be, in principle, obtained from Continuous Global Position System (CGPS), however, since such measurements are still uncertain in the region due to their shortness, limited availability, and noisy character [*Wahl et al*., 2011], we have decided not to use them (note, that the variability within the CGPS time series is usually less than 1–2 cm on a monthly scale, including the seasonal cycle). Instead, and following *Wahl et al*. [2013], we remove only GIA effects from the tide gauge records using the linear VLM trends as calculated by the ICE-5G model (Figure 1a [*Peltier*, [2004]). Given the variety of available GIA models, which may differ significantly from each other at the local scale [*Jevrejeva et al*., 2014], this is a subjective choice. Nevertheless, since the GIA contribution is provided by all models as linear long-term rates of VLMs, using a different model will only affect the trends but not the temporal variability, which is the main focus of this study.

Because historic observations of η_{OBP} (let alone the contribution of the numerous processes affecting η_{OBP}) are not available in the region, here we will assume that, on interannual to decadal time scales, η_{OBP} is dominated by the response of the ocean to changes in atmospheric forcing, and thus its value can be estimated from atmospheric data. This, of course, assumes that the contribution of both VLMs and land-ocean mass exchange to η_{OBP} is small compared to that of atmospheric forcing, and thus can be neglected without introducing serious errors. The validity of this assumption is supported by the fact that 3-D numerical ocean models forced only with wind and buoyancy fluxes can often capture the interannual and decadal sea level variability (corrected for the IBE) at tide gauge locations quite well [e.g., *Carton et al*., 2005; *Stammer et al*., 2013; *Calafat et al*., 2014, Figure 2a], despite missing the contribution of both VLMs and water mass exchange between land and the ocean (their contribution to the coastal MSL variability in the North Sea is suggested to be comparably small (roughly in a similar order as the variations of the global mean (A. Slangen, personal communication, 2014)), which is less than one tenth of the variability of local MSL [*Wahl et al*., 2013]). It follows from our assumptions that η_{OBP} and η_{SLP} are then both a function only of atmospheric forcing, and thus it is convenient to combine them into a single term,

$$\eta_{atm} = \eta_{OBP} + \eta_{SLP} \tag{3}$$

A simplified equation for the local MSL can then be written as

$$\eta_{local} = \eta_{atm} + \eta_{steric} \tag{4}$$

Therefore, here we focus on the contributions of atmospherically induced MSL variations η_{atm} and steric variations η_{steric} (as determined by equation (2)), which can be either locally or remotely driven. It is also important to note that strictly speaking variations in the SSH from altimetry only coincide with the MSL measured by the tide gauges if the sea floor has no vertical motion. However, since the contribution of VLMs on interannual to decadal time scales is relatively small, here we will assume that variations in altimetric SSH and local MSL are comparable.

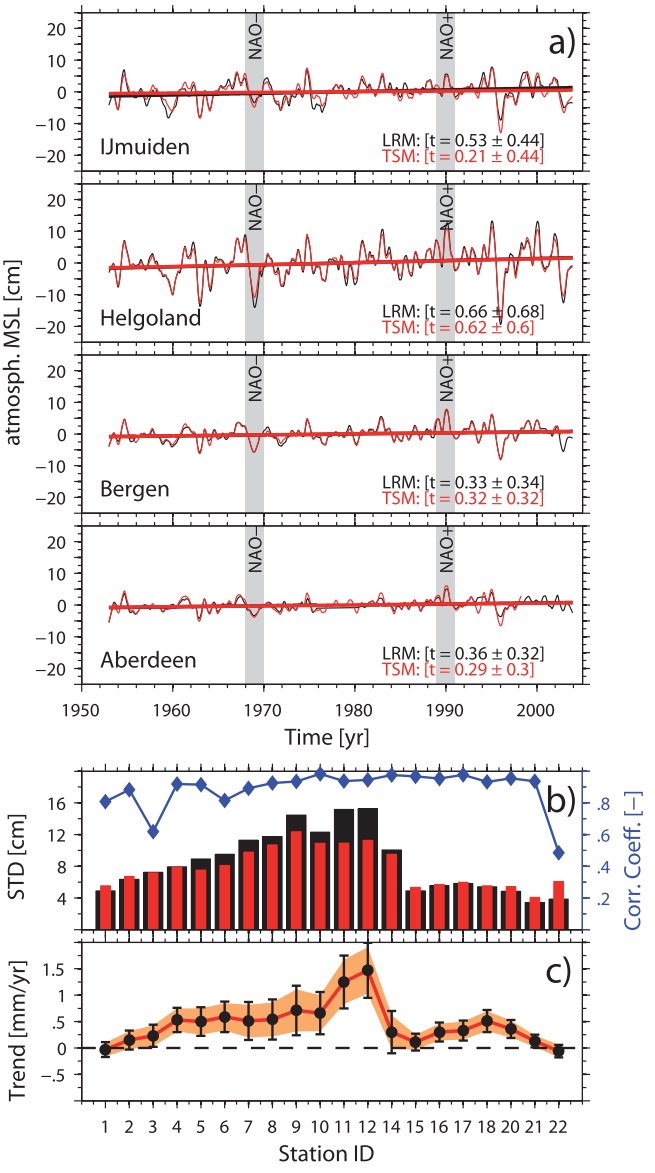

Figure 2. Comparison of the multiple LRM with a state of the art barotropic TSM [*Chen*, 2014] over the period from 1953 to 2003. (a) Four examples for time series and their linear trends of the atmospheric contribution to MSL, η_{atm}, at the locations of Ijmuiden, Helgoland, Bergen, and Aberdeen, respectively. For presentation purposes, all time series have been low-pass filtered with a 12 months moving average filter. The 2 years in which the NAO had its maximum and minimum are marked in gray. (b) Comparison between standard deviations of the atmospheric contribution at different locations estimated with the multiple LRM and the TSM. The correlations between both estimates are shown by the blue diamonds. (c) Comparison of linear trends, including their SEs shown as error bars and shading, respectively. In all subplots, results of the multiple LRM are shown in black, while the results of the TSM are presented in red. Note that only those records have been regarded, where at least 75% of data were available during the investigation period.

To determine η_{atm}, we use a stepwise LRM as introduced by *Dangendorf et al*. [2013a] for the tide gauge in Cuxhaven. Detrended monthly local MSL anomalies are taken as a dependent variable, and detrended zonal/meridional wind stress and SLP anomalies as predictors. Time series of the atmospheric predictors are selected for each tide gauge among the grid points within an area of ±4° around the tide gauge as those with the highest linear correlation with the local MSL from the tide gauge record. Then we apply a stepwise procedure with forward selection, where one by one the predictors giving the highest linear correlation to the MSL record are included into the model until none of the remaining variables significantly improves the model performance (95%-confidence level with f-statistics). The variance explained by η_{atm} (or each other contribution) at each tide gauge is measured by [*Von Storch and Zwiers*, 1999]:

$$VAR_{\exp} = \left[1 - \frac{\mathrm{var}\,(\eta_{local} - \eta_{atm})}{\mathrm{var}\,(\eta_{local})}\right] \quad (5)$$

To estimate the contribution of η_{atm} to long-term trends, we assume that the relationship found for detrended time series on interannual time scales also holds on longer time scales and apply the regression coefficients of the multiple LRM to the deseasonalized but nondetrended wind stress and SLP data.

The use of LRMs raises the question of whether they are able to give a realistic estimate of the atmospheric component, comparable to that provided by a barotropic TSM. The main reason for using LRMs is that none of the TSM runs available for the region cover the period prior to the mid-20th century. Here we validate the LRMs for the second half of the 20th century by comparing them with a state of the art HAMSOM TSM [*Chen*, 2014] and apply them in a second step, together with 20CRv2 reanalysis data, to estimate the atmospheric component back to 1871.

The comparison between the LRMs and the TSM is shown in Figure 2. For each tide gauge record, we estimate the atmospheric component using a stepwise LRM with atmospheric fields from the NCEP/NCAR as

input data. The results are then compared with the output of the TSM at the nearest grid point to the tide gauge. The comparison is performed for the locations of Ijmuiden, Helgoland, Bergen, and Aberdeen each of which is located in one of the four subregions (Figure 2a). The LRM and TSM time series agree well with correlations above 0.92 for the four locations. Correlations for all other individual stations are similar to those found for the four selected stations (Figure 2b), with values that are mostly larger than 0.8. Maximum values exceed 0.9 along the coastlines from Netherlands up to Norway, the Shetland Islands and northern Scotland. The only exceptions are Lowestoft and Hoek van Holland where correlation values of 0.49 and 0.62 are found. Since all surrounding stations compare well, local inaccuracies in the TSM may explain the discrepancies at these two sites. This suggestion is supported by the fact that in both cases, the LRM estimates show significantly higher correlations (Hoek van Holland: 0.78, Lowestoft: 0.58) to the observed time series than the TSM estimates (Hoek van Holland: 0.63, Lowestoft: 0.41). Comparing the standard deviations of the time series from both models, we also find good agreement (Figure 2b). Slightly larger standard deviations originate for the LRM estimates at stations located in the German Bight. There are a number of reasons that may explain these discrepancies: (i) topographic model inaccuracies in the TSM; (ii) local wind variations, which are often linked to changes in large-scale atmospheric circulation and included in the LRMs as remote effects (e.g., changes over the North Atlantic) but not captured by the TSM due to its regional boundary conditions; (iii) changes in atmospheric forcing causing not only barotropic effects but also density variations. Density-related MSL changes may of course be partly captured by the LRM but not by the barotropic TSM. It is difficult to determine which of these reasons is responsible for the differences between the LRMs and TSM. Nevertheless, overall the LRMs agree very well with the TSM, and so it is reasonable for our purposes. Moreover, the agreement is also good in terms of the linear trends (Figure 2c), which further demonstrates that the LRMs are well suited for a long-term assessment in the North Sea.

Linear trends in MSL are estimated using ordinary least squares regression (OLS). Since the residuals of the linear regression model usually contain positive serial correlation, the OLS standard errors underestimate the true standard errors (SE) and thus need to be adjusted. The presence of serial correlation is mostly related to the inertia of the thermosteric component and does not affect the time series of the atmospheric component whose behavior is almost stochastic in nature without any significant correlation structure in the residuals. This is confirmed by an independent Durban-Watson-Test [*Durbin and Watson*, 1951] applied to the atmospheric component at each location (not shown). Hence, whenever the steric component is included in the model, we assume that the residuals follow an autoregressive model of order 1 (AR1) and correct the SE for serial correlation by reducing the degrees of freedom as described by *Santer et al*. [2000]. In cases where only the atmospheric component is analyzed, the SEs directly estimated from OLS are used.

3. Results and Discussion

3.1. The Atmospheric Contribution

The local MSL time series, after the removal of GIA effects estimated with the model of *Peltier* [2004], are characterized by large (up to $\pm$60 cm) intra-annual to decadal variability (Figure 1b). Comparing the different tide gauge records, the decadal-scale variability is similar amongst sites, while the higher frequency fluctuations show considerable differences. Hence, this suggests that the driving factors for the decadal component have a common origin at all tide gauge sites, while different contributing factors influence the higher frequency fluctuations observed across the study area. In the high-frequency bands (i.e., intra and interannual), the records along the Norwegian and UK coastline exhibit a slightly smaller variability, while along the southern coastlines, the variability increases consistently moving eastward, reaching a maximum in the German Bight, a finding consistent with that of *Wahl et al*. [2013].

To investigate these features in more detail, we first compare the local MSL variability to different contributions related to atmospheric forcing, i.e., SLP and wind stress. Figure 3 shows the anomalies of the four regional virtual station time series and the SLP and wind stress anomaly patterns related to phases of particular high ($>$two standard deviations) minus particular low ($<$two standard deviations) local MSL. Large local MSL values in the first two regions (i.e., the southwestern and the southeastern part of the North Sea) are characterized by a pronounced north-south pressure gradient with two anomaly centers of action over Scandinavia and the northeast Atlantic/Iberian Peninsula. This pressure gradient is consistent with a stronger than normal northwesterly flow, resulting in enhanced winds over the southeastern North Sea. The

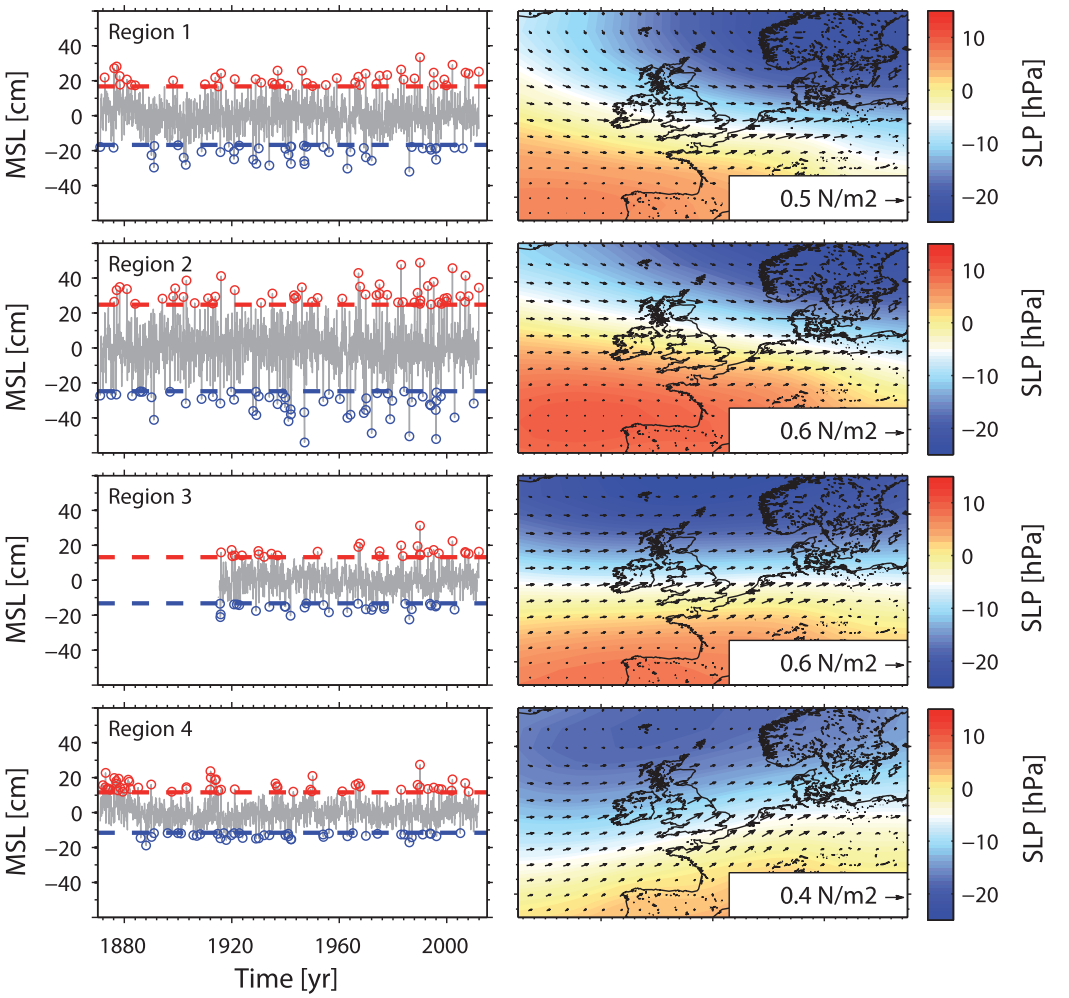

Figure 3. Composite plot for (right) monthly mean SLP and wind stress during times of particularly high (>two standard deviations, red circles) minus particularly low (<two standard deviations, blue circles) (left) monthly local MSL events. The plots are given for the virtual stations of four subregions as defined in section 2.

pattern resembles the Northern Scandinavian Iberian Peninsula Index (NSCI) as introduced by *Dangendorf et al.* [2013b, 2014] and points to a dominant role of westerly winds in the region. The pattern shows similarities to the NAO, but its northern center of action is shifted from southern Iceland toward northern Scandinavia. The dominant zonal winds over the North Sea appear as westerly longshore winds along the southern coastlines. Because of the Ekman transport induced by the longshore winds toward the southern coasts and its resulting convergence of water mass on these coasts, the wind is likely to be more important in these two regions. This is consistent with recent investigations at the Cuxhaven tide gauge [*Dangendorf et al.*, 2013a].

For regions 3 and 4, i.e., the Norwegian and the UK coastlines (see also section 2.1), a pressure gradient is also obvious. However, compared to the first two regions, for the Norwegian tide gauge records, a more meridional pressure gradient over the North Sea leads to a stronger westerly to southwesterly flow. Furthermore, the SLP anomalies in the region are more pronounced and the dominant winds appear cross shore, suggesting that the IBE is little more important in this area in relation to the southern parts of the North Sea. For region 4, the SLP anomalies also show a strong north-south gradient but its northern center of action is more similar to that of the NAO. The lowest anomalies are found over southern Iceland and the wind pattern shows a stronger southwesterly direction, consistent with the imprint of strong NAO+ conditions. Similar to the Norwegian tide gauges, the manifestation of SLP anomalies along the English coast are more pronounced, and wind anomalies face away from the coast. Overall, the composites point to an

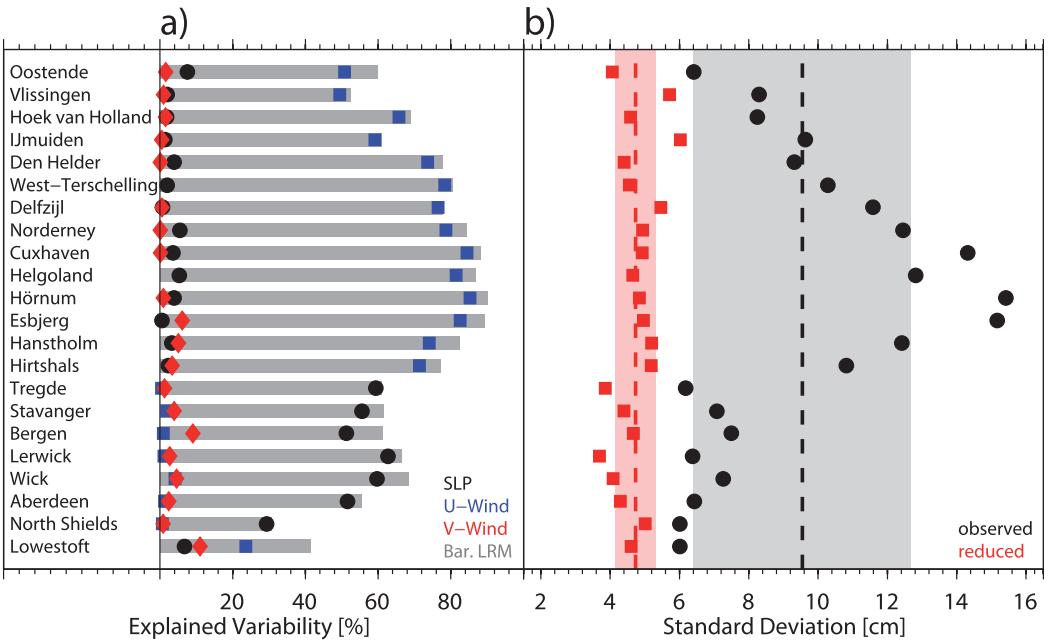

Figure 4. (a) Explained variability by linear regressions between local detrended MSL at different tide gauges around the North Sea coastlines and different local atmospheric forcing factors as well as their combined contribution (barotropic LRM, gray bars). Only predictors explaining a significant fraction of variability are shown (95% confidence level). (b) Intra-annual deseasonalized standard deviations of observed local MSL and atmospherically corrected MSL. The means of intra-annual deseasonalized standard deviations of all gauges are shown by the thick dotted lines together with their interstation standard deviations.

important influence of local atmospheric forcing on the intra and interannual local MSL variability; this is in agreement with earlier studies [e.g., *Tsimplis et al.*, 2005].

The output of the LRMs allows a more detailed analysis of the processes described above and their contribution to the observed local MSL variability. Figure 4a shows the results expressed as explained variability at each individual location. Local atmospheric forcing accounts for most of the observed variability at virtually all stations. The largest contribution is found in the German Bight at the tide gauges of Hörnum and Esbjerg, where atmospheric forcing explains over 90% of the variability. The amount of explained variability clearly follows the observed variability gradient along the coastline discussed above. It increases from values around 60% near the English Channel to over 90% in the German Bight and decreases along the Danish coastline to values around 60% at the Norwegian sites. At the eastern coast of the UK values between 30 and 70% are also observed, with lowest values at Lowestoft and North Shields.

Comparing the individual contributions of SLP and zonal and meridional wind stress (Figure 4a) confirms the results presented as composite plots in Figure 3. While in the northern parts of the Norwegian coast and the eastern UK coastline, SLP dominates the atmospherically induced local MSL variations, zonal winds are more dominant along the southern coastlines from Belgium up to Denmark. At some stations along the UK and Norwegian coastlines, the meridional wind stress component gives a nonnegligible contribution, which is consistent with the wind stress anomalies (and a resulting Ekman transport toward/away from the coast) shown in Figure 3. The results further confirm numerical modeling studies, also pointing to a two-tier system with an IBE dominated region spanning from the English Channel diagonal through the North Sea up to Norway [e.g., *Chen*, 2014].

Figure 4b shows the standard deviations of local MSL η_{local} and the atmospherically corrected time series η_{local} minus η_{atm}. Again, a pronounced variability gradient with up to 3 times larger standard deviations in the German Bight is visible. The mean standard deviation across all sites is ~9.5 cm with a deviation of ~3 cm between the individual stations. After removing the atmospheric component, this variability gradient disappears. The mean standard deviation reduces to ~4.5 cm with an interstation deviation of only ~0.5 cm, reflecting the fact that atmospheric forcing explains most of the variability gradient and accounts for a major part of the background noise in the local MSL time series. Removing the atmospheric

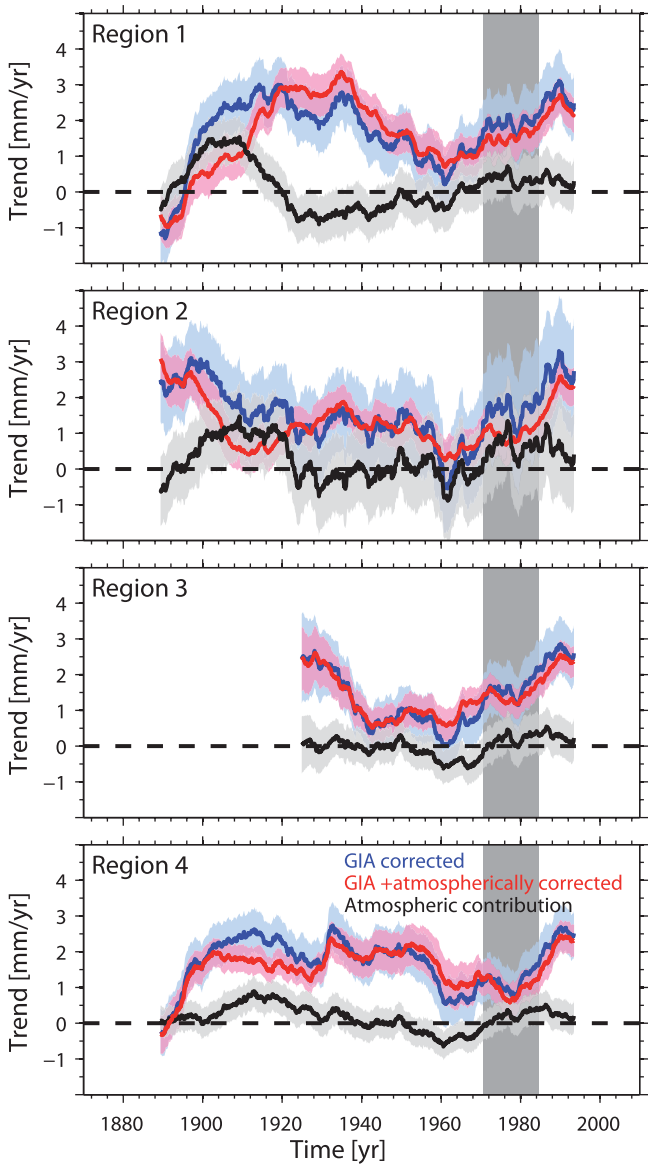

Figure 5. Moving linear trends (37 years) for the observed MSL (blue), the barotropic component of atmospheric MSL (black), and the atmospherically corrected MSL (red) for four different virtual stations corresponding to regions 1–4, respectively. The gray shaded vertical bar marks the period for which the atmospheric (barotropic) component has been validated with the HAMSOM TSM.

component, therefore, will result in a more robust estimation of linear or nonlinear trends (in the sense that the residual variance is reduced, which leads to smaller SEs, see also section 3.4).

It is clear from the results presented so far that the barotropic response of the ocean to local atmospheric forcing accounts for a considerable fraction of the observed intra-annual variability. Next, we assess how it affects local MSL on longer time scales, including its contribution to accelerations. For this purpose, we compute moving trends for each component, i.e., for the local MSL, η_{local}, the atmospheric component, η_{atm}, and the atmospherically corrected time series (Figure 5). This was done for the virtual station time series for each region and using a window length of 37 years to account for the lunar nodal cycle which is superimposed on the trends [*Baart et al.*, 2012].

Focusing first on the local MSL component η_{local}, it is obvious that the moving trends alternate between higher and lower rates, with three major features common to all virtual station records: high rates in the early decades of the 20th century, a decrease toward almost zero in the 1960s, and a steady increase afterward. These features were also found by *Wahl et al.* [2013]. The atmospheric component η_{atm} is marked by a phase of relatively large trend rates in the early 20th century and fluctuates around zero afterward. Only in the southeastern North Sea (region 2), a considerable contribution of the atmospheric component to the acceleration in the rate of rise observed in recent decades can be found. This is due to an increase in the atmospheric contribution from the 1960s to the mid-1990s. *Marcos and Tsimplis* [2007] and *Dangendorf et al.* [2012] found that the increase mainly occurred during the winter season and they attributed it to particular strong NAO+ conditions with more frequent southwesterly winds [*Siegismund and Schrum*, 2001]. Removing the atmospheric component from the observations reduces the 37 year trends by up to 1 mm/yr, but leaves the major longer-term features mostly unchanged. Hence, we conclude that local atmospheric forcing is a major contributor to sea level variability on intra and interannual time scales but fails to explain longer-term variations.

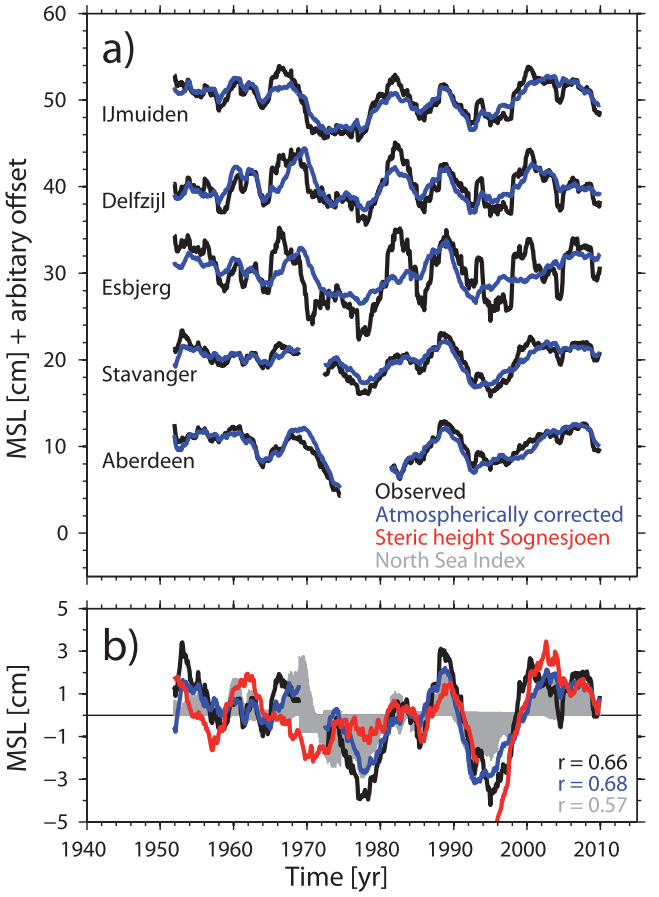

Figure 6. (a) Low-pass filtered (48 months moving average) MSL time series from five representative stations in the North Sea. The black lines represent the observed time series, while the atmospherically corrected time series are shown in blue. (b) The observed and atmospherically corrected MSL record at Stavanger in comparison to the steric height calculated from temperature and salinity profiles at Sognesjoen. The North Sea index (atmospherically corrected; gray area) and linear correlations between all sea level time series and the steric height are also shown.

3.2. Steric Height

Following our assumptions made in section 2 and according to the separation in equation (4), the remaining signal of η_{local} after removing η_{atm} is to large extend determined by η_{steric}. The North Sea has—except in parts of the Norwegian Trench—water depths that are mostly less than 100 m. Along the coast, where most tide gauges are located, water depths are less than 10 m. Since the steric height is commonly computed as an integral over depth, its contribution is negligible if it is calculated in the shallow region over the continental shelf. This, however, does not imply that the variability measured by coastal tide gauges is unrelated to steric changes. In fact such variability is often produced by steric variations in the deep ocean external to the region. For instance, the isopycnals that intersect the continental slope may fluctuate vertically, which will be reflected as mass changes at the tide gauge. To get a measure of the steric contribution to coastal sea level, *Bingham and Hughes* [2012] demonstrated on the basis of an ocean model that for the European Atlantic coast, the best results are obtained when the steric is computed in a depth range of 500–1000 m near the shore.

In the case of the North Sea, one can either use the steric height inshore of the North Atlantic Current, near the northern entrance, or that obtained in the Norwegian Trench. The former is not possible due to the lack of data. However, the permanent station at Sognesjoen provides temperature and salinity data in the Norwegian Trench for the upper 300 m from which the steric component can be calculated. To demonstrate that—at least at longer time scales—the local MSL variability along the southwest coast of Norway near the Norwegian Trench is consistent with that in the North Sea, we have compared the decadal component of local and atmospherically corrected MSL from the Stavanger tide gauge in Norway with that measured in the shallow parts of the North Sea as represented by four stations from the subregions (Ijmuiden, Delfzijl, Esbjerg, and Aberdeen) over the period from 1950 to 2011(see Figure 6a).

The time series of all five stations exhibit similar patterns of decadal variability with values ranging between ±5 cm (this is true for the local and the atmospherically corrected MSL). For example, all locations show a drop in the mid-1960s and a maximum at the end of the 1980s. Figure 6b compares the Stavanger local MSL with the steric height computed from temperature and salinity profiles at Sognesjoen in the Norwegian Trench. The decadal features fit reasonable well with the observed and atmospherically corrected decadal signals from the coastal sea level. This is expressed by high correlations between the steric height and both the observed local ($r = 0.66$) and the atmospherically corrected MSL ($r = 0.68$). The North Sea index is also significantly correlated with the steric height ($r = 0.57$).

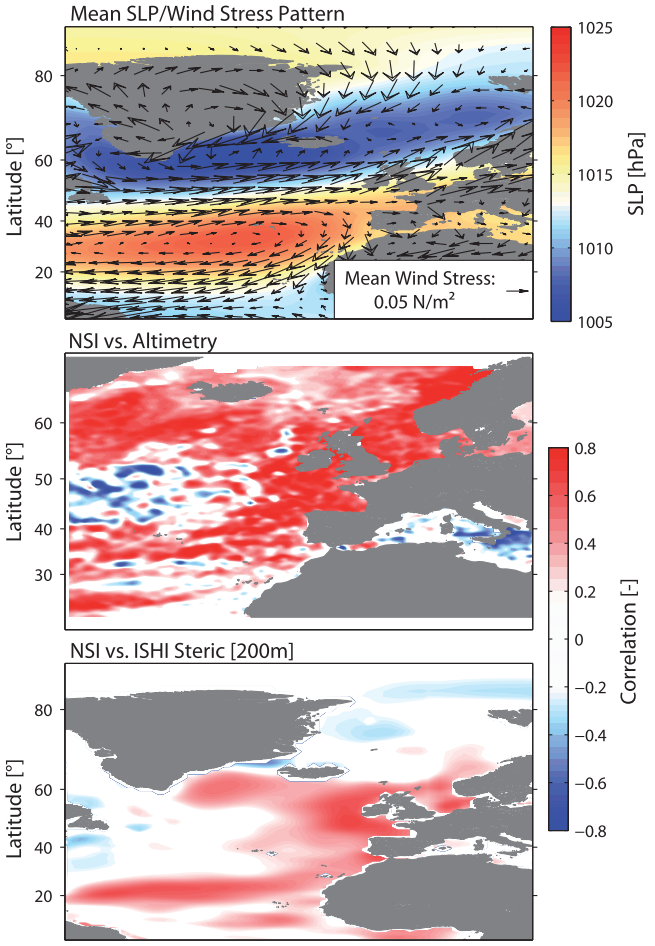

Figure 7. (top) The average SLP and wind stress pattern over the period from 1945 to 2011 as estimated with 20CRv2 data. (middle) Linear correlations between the North Sea local MSL index (atmospherically corrected) and gridded time series of IBE corrected AVISO SSHs over the period 1993–2011, and (botom) steric heights as provided by *Ishii and Kimoto* [2009] over the period 1945–2011.

Our results show that a considerable fraction of decadal scale variability of coastal MSL in the North Sea is—regardless of the question of its geographical origin—driven by steric sea level changes. Given the above mentioned spatial coherence of decadal local MSL variability in the region it can be assumed that temperature and salinity profiles from the Norwegian Trench can provide, at least to some extent, a good estimate of the steric component in the entire North Sea.

3.3. Remote Forcing

The next question we turn to is concerned with the geographical and physical origin of the decadal fluctuations in the region. *Sturges and Douglas* [2011] explored the idea that the multidecadal local MSL variability observed in the tide gauge record at Cascais, Portugal, may be related to changes in longshore winds. They argued that changes in the intensity or direction of the persistently southward blowing winds along the continental shelf produce an ocean response of both barotropic and baroclinic nature with a consequential change in sea level at the coast. Such response is not strictly local due to the possibility that coastally trapped waves may be excited and propagate northward along the coast, thus inducing sea level changes at all points northward of the region where the wind is blowing [*Gill*, 1982]. In order to take the cumulative effect of the wind into account, *Sturges and Douglas* [2011] integrated the longshore wind from the equator up to Cascais. They found a good agreement between the integrated longshore wind and the local MSL at Cascais on decadal time scales, supporting their hypothesis. *Calafat et al*. [2012] expanded these investigations and demonstrated that the link with the longshore wind exists for a large portion of the eastern boundary of the North Atlantic and also for the Mediterranean Sea. With the help of an ocean model they also were able to show that the response of the ocean, responsible for this link, is of baroclinic rather than barotropic nature. In a subsequent study, *Calafat et al*. [2013] used a proxy for the propagating signal of Atlantic origin in combination with local winds over the Norwegian continental shelf to show that such signal can propagate further north into the Norwegian Sea and even in the western Siberian Seas. Using this reconstruction, they were able to explain over 70% of the observed local MSL variability along the Norwegian coast. Whether the signal affects also the North Sea is still an open question which needs to be assessed.

To illustrate possible mechanisms of boundary wave generation in the northeast Atlantic, Figure 7 (top) shows the average atmospheric conditions as estimated from the 20CRv2 wind and pressure fields over the period from 1950 to 2011. The region is characterized by a strong pressure gradient with a low-pressure center in the north and a high-pressure center over the Azores. The resulting wind stress patterns show a clockwise circulation centered on the Azores islands with prevailing (south-) westerlies from the Bay of Biscay northward. It is important to note that, in addition to the waves generated at distant locations

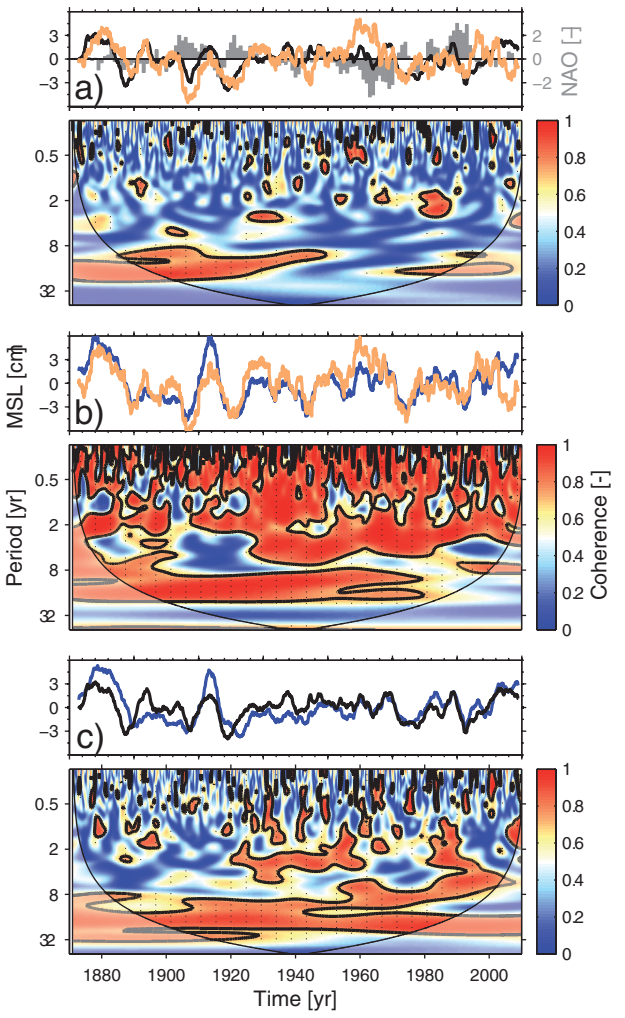

Figure 8. Wavelet coherence between (a) the North Sea index of local atmospherically corrected MSL and longshore winds integrated from 6°N to 55°N, (b) local MSL at Newlyn and longshore winds integrated from 6°N to 50°N, and (c) the North Sea index of atmospherically corrected local MSL and the IBE corrected local MSL at Newlyn. Above each coherence plot, also the corresponding low-pass filtered time series (48 months moving average) are shown (North Sea index MSL: black, Newlyn MSL: blue, longshore winds: yellow). In Figure 8a, the winter NAO index (December to March) from *Hurrel et al.* [2003] is shown by the gray bars. The coherence has been calculated with the default version (Morlet wavelet) of the *Grinsted et al.* [2004] MATLAB wavelet toolbox. To extend the Newlyn record to the entire investigation period from 1871 to 2011, gaps have been filed via linear regression with the PSMSL Brest record, i.e., before 1916 all values are based on Brest data.

[*Calafat et al.*, 2012], the westerlies north of 45°N will generate new waves, and thus the associated sea level changes at higher latitudes can be considered as a superposition of continuously wind-forced coastally trapped waves [e.g., *Gill*, 1982]. It is obvious that the westerlies will also intensify the North Atlantic Current and pile up the water on the North Sea coasts due to Ekman transport. The suggested coherence of decadal variability in the region is demonstrated by correlating the low-pass filtered North Sea index derived from satellite altimetry (2°W to 10°E and 50°N to 62°N) with similarly filtered SSHs from satellite altimetry over the entire Northeast Atlantic area (Figure 7, middle). While the altimetry data are—due to the shortness of the observations—still limited for long-term variability investigations, they provide useful information on the spatial coherence of MSL in the region. The highest correlations are found over the continental shelf areas along the Norwegian coast and along the eastern boundary of the North Atlantic from western UK down to the Canary Islands. This suggests the existence of a coherent signal with a common origin in the North Atlantic and fits with the theory of wave propagation associated with longshore wind forcing. A similar correlation map is obtained when using steric height instead of altimetry data, for the longer period from 1945 to 2011 (Figure 7, bottom), reflecting a predominantly baroclinic behavior of the waves as found by *Calafat et al.* [2012]. This further suggests that wind forcing over the region northward of the Gulf of Biscay is especially important for the generation of local MSL variability in the North Sea.

The link between decadal wind forcing and local MSL in the North Sea, which is suggested to be connected with the position and intensity of the NAO centers of action [e.g., *Jevrejeva et al.*, 2005], is further investigated by comparing the longshore winds integrated from the equator up to higher latitudes. This is achieved (Figure 8) by comparing the time series via wavelet coherence plots [*Grinsted et al.*, 2004]. We find significant coherence between the atmospherically corrected North Sea MSL and the integrated longshore winds in frequency bands of ~8 to 20 years, which is also supported by significant correlations between the time series itself ($r = 0.49$, the number of degrees of freedom was reduced with respect to the smoothing, Figure 8a). However, compared to the local MSL in Newlyn [*Calafat et al.*, 2012], the coherence is lower, more confined to the decadal scales (note that interannual sea level variations in Newlyn are governed by local longshore winds, which are in turn also part of the integrated winds, while in the North Sea other factors are more important as discussed above) and also nonstationary in time (Figure 8b). There are several

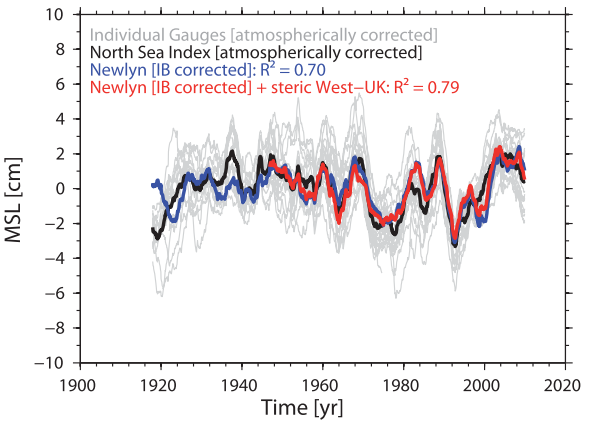

Figure 9. Comparison between the atmospherically corrected local MSL of the North Sea index (black), the IBE corrected MSL at Newlyn (NEWc, blue), and a reconstruction (multiple regression) based on the NEWc and the steric height observed west of the UK. The NEWc is used as a proxy for longshore wind forcing and the resulting wave propagation along the eastern boundary of the North Atlantic [*Calafat et al*., 2012] (see also Figure 8b). Individual North Sea records are also shown (gray). All time series have been low-pass filtered with a 48 month moving average filter.

possible causes for this. First, boundary waves may lose energy through radiation of westward-propagating Rossby waves as they propagate poleward along the coast. As an example, *Marcos et al*. [2013] provided evidence that local MSL at the Canary Islands is correlated with that along the continental boundary, reflecting the propagation of the signal from the coast to the offshore islands is in the form of Rossby waves. This implies that, for tide gauges located at high latitudes, it may be more appropriate to start the integration of the longshore wind from higher latitudes rather than from the equator. Second, coastally trapped waves can scatter strongly due to topographic variations (e.g., shelf width changes). Finally, inaccuracies in the wind data due to the lack of wind observations over the ocean may also contribute to the relatively low correlation between integrated longshore wind and steric MSL at high latitudes.

Hence, due to these limitations and following *Calafat et al*. [2013], we decided to use local MSL data from the tide gauge record at Newlyn (UK, note that for the wavelet analysis gaps were filled using a linear regression to the Brest record (r = 0.94)) instead of winds themselves as a proxy for the propagating signal of Atlantic origin. The wavelet analysis of the IBE corrected Newlyn time series and the atmospherically corrected North Sea MSL index points to a more coherent and stationary relationship on decadal scales (Figure 8c), which is also supported by the low-pass filtered time series shown in Figure 9. Both time series show remarkable similarities with a correlation of ∼0.84. In total, ∼70% of the decadal-scale variability in the North Sea can be explained by the propagating signal of Atlantic origin alone. The correlation patterns with the steric height in Figure 7 further suggest that the regions north of Portugal and west of the UK are the most relevant to the generation of decadal MSL variability in the North Sea. As a complementary analysis, we combined (in a multiple regression) the tide gauge record at Newlyn with the steric height west of the UK (352°W: 52°N) and compared it to the North Sea index (Figure 9). This further improves the model resulting in a linear correlation of 0.89 and an explained variability in the order of ∼79%. These results demonstrate that a significant fraction of the decadal variability is related to remote forcing over the North Atlantic.

3.4. Implications for the Estimation of Trends and Acceleration Patterns

We are not only interested in understanding the different physical processes controlling local MSL variability in the North Sea but also in the influence of known variability to linear trends and acceleration/deceleration patterns. *Dangendorf et al*. [2013a] demonstrated (for the sea level record measured at the tide gauge of Cuxhaven) that the atmospheric contribution η_{atm} strongly influences its noise characteristics. Since the noise determines the SE of a linear trend, removal of known parts reduces the residual variance leading to smaller former trend uncertainty. Please note that this should ideally been done with the detrended atmospheric MSL, η_{atm}, unless one is also interested in trends of the internal variability. *Dangendorf et al*. [2013a] showed that lengths of 50–60 years are required to obtain SEs in the order of 0.5 mm/yr, at Cuxhaven. After removing η_{atm}, the required lengths reduced to ∼30 years (a value comparable to those obtained at other tide gauges around the globe [*Douglas*, 1991]).

Here we carry out a similar analysis for each of our tide gauge locations in the North Sea. In the procedure applied by *Douglas* [1991] and *Dangendorf et al*. [2013a], the observed records were used to estimate the SE in relation to the time series length by determining the linear trend and its SE for different window lengths starting with a window centered on the last 19 years and subsequently increasing the window length year

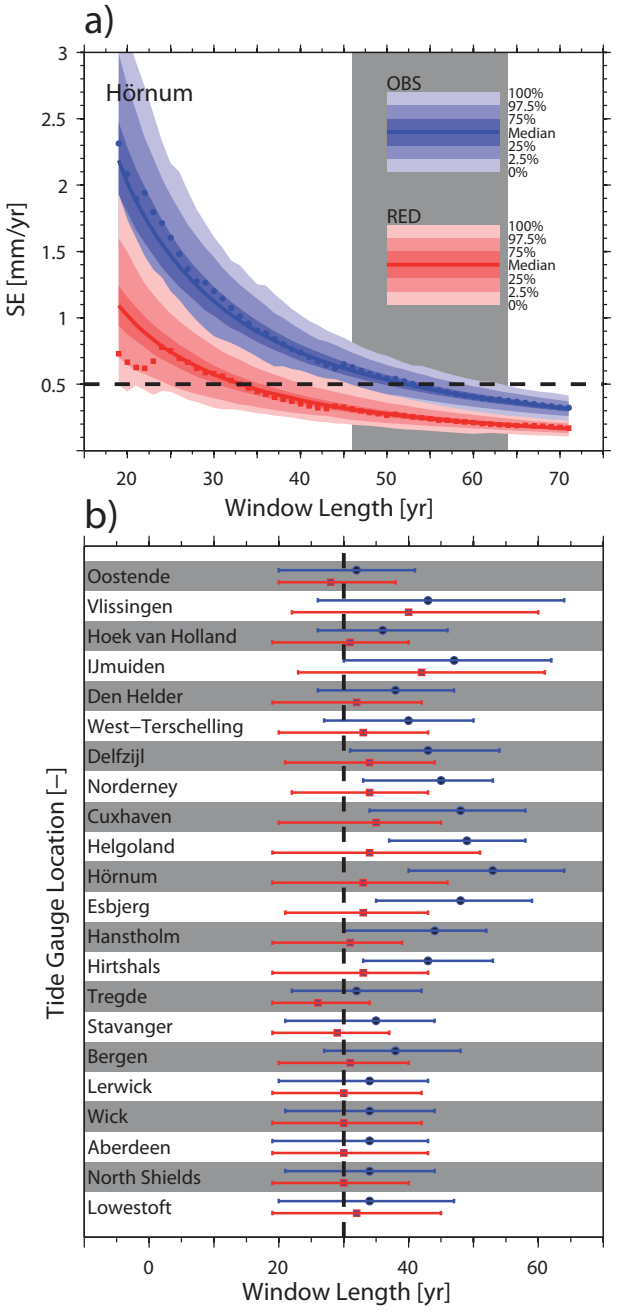

Figure 10. (a) The SE as a function of time series length for observed local (blue dots) and atmospherically corrected (red dots) MSL time series at the tide gauge of Hörnum. For both time series sets, AR(1) models are used to simulate a set of 1000 artificial time series with realistic noise. The blue and red shaded areas represent the range of SEs estimated from the 1000 simulations. The black dotted line shows a SE of 0.5 mm/yr, a value that is typically as associated with "robust" linear trend estimations. The gray shaded area marks the reduction that is reached through the atmospheric correction. (b) Median (dots) and maximum/minimum range (lines) of SEs derived from the simulations used for (Figure 10a) observed (blue) and atmospherically corrected (red) time series at all stations. The black dotted line shows the 30 year window length, often needed to achieve a SE $<$ 0.5 mm/yr [e.g., *Douglas*, 1991].

by year back in time. This procedure is somewhat arbitrary since the SE strongly depends on the structure of the background noise in the respective time series window (note that also the variance of the MSL time series is non-stationary). To get a more general expression of the dependence of the SE on the time series length, we conduct a Monte-Carlo experiment, in which we first estimate an AR1 model for each entire tide gauge record with the parameters a (noise variance) and g (lag-1 autocorrelation). These parameters are then used to simulate a set of 1000 artificial time series with noise typical for each of the considered tide gauge records by following the approach given by *Allan and Smith* [1994]. The artificial time series are used to get a more robust estimate of the length required for the estimation of linear trends with a certain degree of accuracy, i.e., the SE is measured for different time series lengths 1000 times. This is done for 1000 time series containing noise typical for the local MSL, η_{local}, as well as 1000 time series with noise characteristics typical for the local MSL corrected for the atmospheric contribution η_{atm} (only the barotropic term).

Figure 10a exemplarily shows the results for the tide gauge record at Hörnum. For the local MSL, $\sim 52 \pm 10$ years (uncertainties estimated with the percentiles of the artificial time series) are required to estimate a linear trend with a SE in the order of 0.5 mm/yr. If the atmospheric contribution, η_{atm}, is removed from the time series this value is reduced to $\sim 33 \pm 10$ years (95% confidence), highlighting the benefit of removing known variability from noisy time series before calculating trends.

Figure 10b shows the number of years required to obtain SEs in the order of 0.5 mm/yr for both components, i.e., the local MSL and the atmospherically corrected MSL, for all study sites. As expected from the variability analyses described before, longer time series

are required to achieve a moderate SE in the southeastern parts of the North Sea basin, compared to the other regions. When applying the atmospheric correction, the number of years required to estimate the linear trend with the desired accuracy reduces to ~30 years, a number that is similar to the length reported by *Douglas* [1991] who analyzed selected records from tide gauges around the globe.

Finally, we examine to what extent the atmospheric correction can improve the detection of acceleration/deceleration patterns, which is of particular relevance when searching for a possible increase in the rate of SLR of anthropogenic origin. To do this, we follow the methodology proposed by *Haigh et al*. [2014], i.e., we artificially extend tide gauge records to 2100, by combining future projections of SLR with realistic interannual variability. We then calculate 37 year moving trends and detect the years in which a significant (95% confidence) acceleration first becomes evident. We combine four different projections (Figure 11a), two based on the IPCC's AR5 report [*Church et al*., 2013, hereafter P1 (0.50 m) and P2 (01.00 m), respectively] (they correspond to the low and upper range of the Representative Concentration Pathway (RCP) 8.5, which correspond approximately to 0.5 and 1 m SLR by 2100, relative 1986–2005) and two accounting for higher values as estimated with semiempirical models [e.g., *Rahmstorf et al*., 2007; *Moore et al*., 2013, hereafter P3 (1.5 m) and P4 (2.0 m), respectively]. To all projections, we add artificial noise (1000 time series, to account for uncertainty in future variability) from the AR1 model described above. Again, this is done for the local MSL and the atmospherically corrected MSL. For illustration, we present results for three selected tide gauges (Delfzijl, Esbjerg, Cuxhaven), which are: (i) long enough (i.e., covering the 20th Century) and (ii) contain a considerable fraction of atmospherically induced variability. We compute 37 year moving trends over the entire time series (observation + projection), identify the largest rate within the observations and search for the earliest period in the projections, in which five consecutive years exceed the maximum rate from the observations by taking into account their confidence intervals (Figure 11b). The last year of the 37 year period for which this criterion is fulfilled is assumed to be the "detection point" at which we are able to tell that there is a significant acceleration. If no significant acceleration can be detected, the detection point is >2100.

The results for each of the three tide gauge records are shown in the box plots of Figure 11c. According to *Haigh et al*. [2014] for the lowest scenario of 0.50 m SLR until 2100, the detection of a significant acceleration is a nontrivial task, as in a considerable number of simulations no significant acceleration can be detected before 2100. The median value of all simulations for P1 is 2061 (95% percentiles: 2035->2100), >2100 (2075->2100), and >2100 (2054->2100) for the locations of Delfzijl, Esbjerg, and Cuxhaven, respectively. The higher the SLR projection, the earlier a significant acceleration can be detected. With the exception of P2 at the locations of Esbjerg and Cuxhaven for all remaining projections, a significant acceleration is detected at all sites. If noise typical for the atmospherically corrected MSL is applied, the detection performance increases considerably, resulting in median values of 2050 (2029–2074) for Delfzijl, 2060 (2031->2100) for Esbjerg, and 2062 (2040->2100) for Cuxhaven. Under the assumption of the highest projection P4, median values of 2020 (2019–2026), 2025 (2019–2038), and 2022 (2019–2030) for time series with noise typical for local MSL and 2020 (2019–2025), 2021 (2017–2028), and 2022 (2019–2028) for time series with noise typical for atmospherically corrected MSL are calculated at the three stations. These results show that the detection of possible accelerations on a regional scale as considered here, strongly depends on the signal to noise ratio of the investigated time series. Atmospheric forcing might mask possible anthropogenic signals related to, for instance, global warming of the oceans or accelerated meltwater discharge. As an example, *Calafat and Chambers* [2013] have recently shown that internal climate variability can contribute by up to 97% (depending on the location) to local MSL accelerations at numerous tide gauges from around the world. By removing this contribution, they were able to detect a statistically significant acceleration in coastal MSL between 1952 and 2011, which was related to external forcing (both anthropogenic and natural). Clearly, removing known patterns of variability from time series of local MSL enables earlier detection of possible underlying signals due to external forcing factors.

4. Conclusions

An assessment of MSL variability and its forcing across a range of different time scales has been undertaken for 22 tide gauge records in the North Sea; nine which extend back to the late 19th century. The North Sea is one of the best instrumented regions worldwide and is therefore of particular importance for global MSL reconstructions [e.g., *Jevrejeva et al*., 2005; *Church and White*, 2011; *Jevrejeva et al*., 2014]. Our analysis suggests considerable intra-annual to decadal-scale variability superimposed on well-known long-term trends

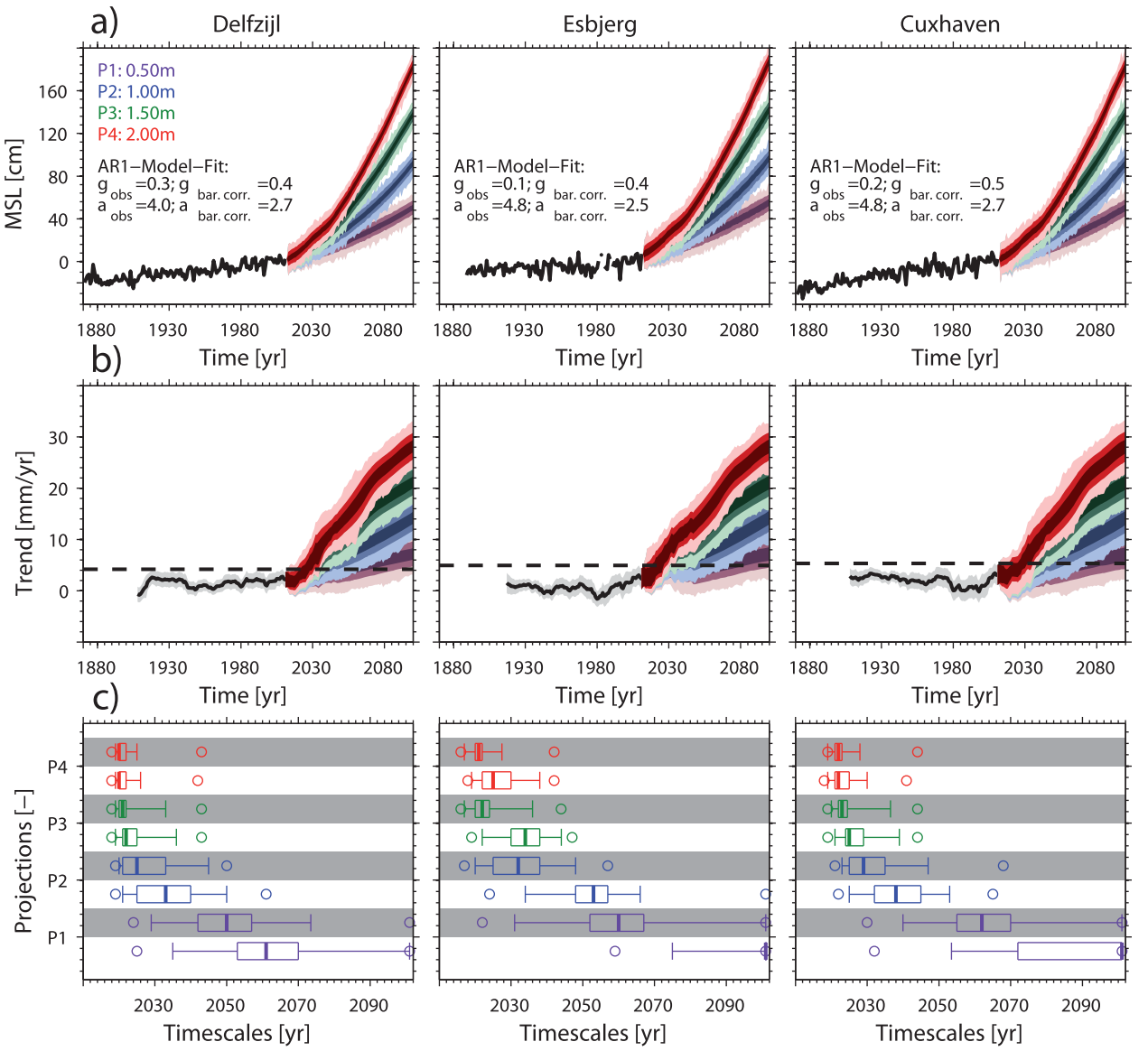

Figure 11. (a) Observed annual local MSL (black, corrected for GIA) for three different locations together with four artificial projections (P1, P2, P3, P4). Each projection is combined with 1000 time series of artificial noise, as simulated on the basis of an AR1 model. The different color shades contribute to different percentiles (100, 95, 75, 50, 25, 5, 0) of the 1000 artificial time series per projection. Estimates of the two AR1 parameters, g (lag-1 autocorrelation) and a (noise variance), are also shown. (b) The 37 year moving trends for the observations (black and gray shading) and as estimated with the different artificial projections. Again the color shade is related to the percentiles of the full set of 1000 time series. (c) Boxplots (100, 95, 75, 50, 25, 5, 0) of the years in which a significant acceleration can be detected for the four different projections relative to the historic observations. The white shading marks the results using realistic noise for the observed local MSL time series, while the gray shading represents the boxplots for realistic noise based on time series, which have been corrected for local atmospheric forcing.

[*Wahl et al.*, 2013]. The largest intra to interannual variability (up to ±60 cm) is found in the southeastern part of the North Sea, which is up to 3 times larger than elsewhere in the region. On decadal time scales, the variability is more coherent in magnitude throughout the region.

The variability on time scales ranging from months to a few years is dominated by atmospheric forcing and related barotropic adjustment processes in the ocean. However, the physical mechanisms driving the variability are different across the region. There is a transverse line from the English Channel to Norway separating the North Sea into two distinct regions with different characteristics [*Chen*, 2014]. In the northern parts, the largest deviations around the mean are caused by the IBE. Here wind plays only a secondary role. In the southeastern parts, the situation is reversed and the wind contributes to the majority of the variability. Generally, the North Sea region is characterized by a meridional pressure gradient leading to prevailing

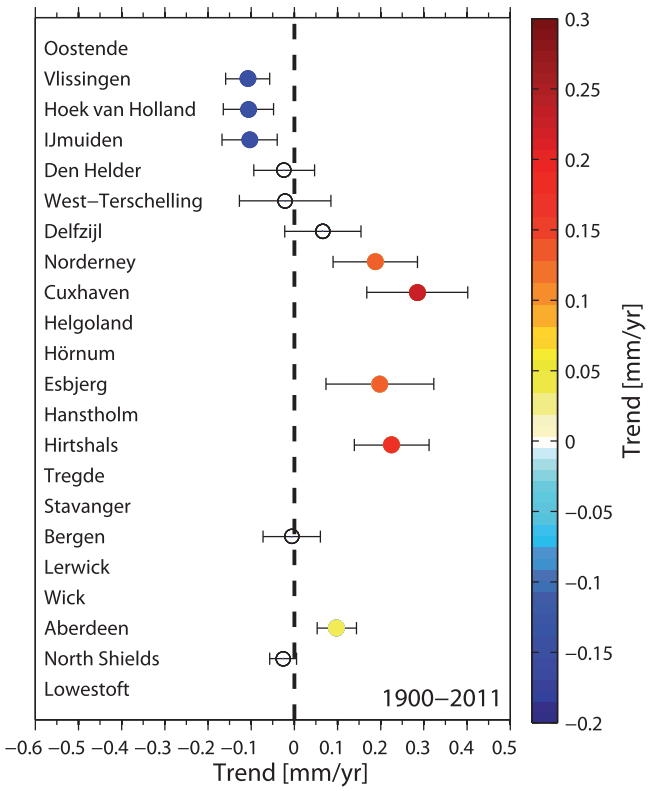

Figure 12. Linear trends and their SE (95% confidence level) of the atmospheric contribution, η_{atm}, to local MSL over the period 1900–2011. Only those trends are shown, where at least 75% of the data were available. Colored dots represent trends which are statistically significant on the 95% confidence level.

westerlies, acting as longshore winds along the southern coastline and piling up the water masses in the shallow southeastern parts of the basin [see also *Wakelin et al*., 2003].

The large influence of atmospheric (barotropic) forcing on the shallow continental shelf area decouples the North Sea on intra and interannual time scales from surrounding areas, resulting in low correlations, for example, with stations in the English Channel [*Wahl et al*., 2013]. On decadal time scales, on the other hand, the coherence between the different stations in the basin is much higher (suggesting a common forcing mechanism) and the barotropic response of the ocean to local SLP and wind stress forcing becomes negligible. Since the North Sea is mostly shallow (with water depths below 100 m), the steric height calculated locally can also not account for the remaining fluctuations. Therefore, we have estimated the steric component exemplary for the Norwegian Trench, where the water depth is large enough to give a significant steric signal. We found that the variations in the steric height agree well with the local MSL especially on longer time scales. Given the spatial coherence on these time scales, we conclude that this result can be taken to be representative for the entire basin. The question that remains is where these steric MSL changes are triggered?

To answer this question, we have explored the coherence of North Sea MSL on decadal scales with the surrounding seas and found a band of coherent MSL variability extending from the Norwegian coastline along the eastern boundary down to the Canary Islands. This coherency suggests a common forcing and fits well with the theory of longshore winds as also proposed in recent studies by *Sturges and Douglas* [2011], *Calafat et al*. [2012, 2013], [*Calafat and Chambers*, 2013], and *Marcos et al*. [2013]. These longshore winds cause a displacement of the thermocline leading to coastally trapped waves which propagate with the coast on the right (in the northern hemisphere) further northward. Complementary to the above mentioned studies, we find evidence that the signal propagates on its way north into the North Sea region. Generally, the waves appear to be caused in the region south of 45 N by changes in the strengths of the prevailing anticyclonic circulation (around the Azores High) [e.g., *Sturges and Douglas*, 2011]. Our results imply that the decadal local MSL variability in the North Sea represents a combination of propagating waves triggered at different latitudes. For instance, the highest dependencies are found between the atmospherically corrected North Sea MSL and the steric height in the Gulf of Biscay and especially the region west of the UK. As previously described, e.g., by *Orvik and Skageseth* [2003] and *Richter et al*. [2009], the inflow of Atlantic waters into the Nordic Seas is strongly governed by low-pressure systems with prevailing westerly to southwesterly winds and subsequent baroclinic adjustment processes in the ocean. If we combine the IBE corrected local MSL in Newlyn with the steric height west of the UK, we can explain ∼79% of the decadal variability demonstrating the dominance of the propagating signal on decadal and multidecadal time scales.

The origin of this variability has important implications for developing future MSL projections in the region, since the signals described in the present study are superimposed onto the longer-term changes. Such

decadal-scale fluctuations can cause coastal MSL to exceed a certain threshold, even only for a few years, much earlier than the time expected for the global mean to cross the same threshold. Additionally, due to the coarse resolution of the ocean component, most global climate models in the AR5 are not able to resolve the described processes on the shallow continental shelf. Given the mostly baroclinic nature of the signal with a Rossby radius of about 20km or less [*Gill*, 1982], it is clear that the zonal resolution of the most models (1 (∼100 km) or larger) is too coarse. Hence, statistical or dynamical downscaling techniques [e.g., *Von Storch et al*., 1993; *Dangendorf et al*., 2013b] may represent a valuable tool to overcome these resolution problems. The finding that the decadal-scale variability in the North Sea has its origin (at least partly) in baroclinic adjustment processes of the ocean in the North Atlantic further gives important information on the boundary conditions for the regional models generally used for dynamical downscaling.

Besides their influence on the temporal variability, it is also of interest to examine how much the local atmospheric component contributes to 20th century MSL trends at each site (Figure 12). The atmospheric component, η_{atm}, shows local differences up to 0.4 mm/yr between the individual sites (Figure 12). *Wahl et al*. [2013] also pointed to distinctive spatial differences in rates of SLR in the North Sea and suggested that these were mainly related to uncertainties in the estimates of VLMs. The results presented here show that local atmospheric forcing also affects the spatial trend patterns of local MSL and should therefore be removed before any VLM analysis in the region.

We further analyzed the role of local atmospheric forcing on the estimation of long-term trends and acceleration/deceleration patterns using a combination of observations and a set of artificially generated time series. The important finding from these analyses is that atmospheric forcing (dominating local MSL variability on intra and interannual time scales) is the main factor controlling the signal to noise ratio in the time series. This has two significant implications:

1. The accuracy of the linear long-term trend strongly depends on whether the atmospheric correction has been applied or not. Removing known parts of variability leads to more robust trend estimates and hence shorter time series can be included in studies focusing on long-term trends. This finding is most relevant for areas where only short records exist [see also *Dangendorf et al*. 2013a]. The effect of removing the known variability in the North Sea is largest in the wind-dominated areas, where the interannual variability is more pronounced.
2. The removal of atmospherically induced MSL variations increases the signal to noise ratio and therefore allows earlier detection of possible SLR accelerations (here up to 40 years depending on the location and the projection and compared to using uncorrected time series), as projected under a warming climate.

The later point is important for coastal planning and safety management. Today anthropogenic climate change represents one of the major global challenges and coastal societies are discussing major investments in order to adapt to climate change. Local authorities need to know as early as possible how much SLR is likely to be expected over the next decades in order to prevent coastal flooding. The earlier we identify which climate change pathway the Earth's climate system is following and how much SLR might be expected, the better we can adapt to it. Hence, we strongly recommend applying the atmospheric correction to the data in the region before estimating linear trends or possible accelerations.

Acknowledgments

We acknowledge Xinping Chen and Thomas Pohlmann from the University of Hamburg for providing us the outputs of the HAMSOM model. Thanks to Birgit Klein for the fruitful discussions. F. M. Calafat was supported under a Marie Curie International Outgoing Fellowship (IOF) within the 7th European Community Framework Programme (grant agreement number PIOF-GA-2010-275851). T. Wahl was supported by a fellowship within the postdoctoral program of the German Academic Exchange Service (DAAD). I. D. Haigh was supported by the UK Natural Environment Research Council iGlass consortium project (NE/I009906/1). All the data used in the present study can be found on the web pages referenced in the text. We further thank the Twentieth Century Reanalysis team for providing the data set without any charge. Support for the Twentieth Century Reanalysis Project data set is provided by the U.S. Department of Energy, Office of Science Innovative and Novel Computational Impact on Theory and Experiment program, and Office of Biological and Environmental Research, and by the National Oceanic and Atmospheric Administration. All data sets used in the present study, except the numerical model outputs, are online available from the webpages cited in section 2.2.

References

Albrecht, F., and R. Weisse (2012), Pressure effects on past regional sea level trends and variability in the German Bight, *Ocean Dyn.*, *62*, 1169–1186, doi:10.1007/s10236-012-0557-1.

Allan, M. R., and L. A. Smith (1994), Investigating the origins and significance of low-frequency modes of climate variability, *Geophys. Res. Lett.*, *21*, 883–886.

Amos, C. B., P. Audet, W. C. Hammond, R. Bürgmann, I. A. Johanson, and G. Blewit (2014), Uplift and seismicity driven by groundwater depletion in central California, *Nature*, *509*, 483–486, doi:10.1038/nature13275.

Baart, F., P. H. A. J. M. van Gelder, J. de Ronde, M. van Koningsveld, and B. Wouters (2012), The effect of the 18.6-year lunar nodal cycle on regional sea level rise estimates, *J. Coastal Res.*, *28*, 511–516.

Bingham, R. J., and C. W. Hughes (2012), Local diagnostics to estimate density-induced sea level variations over topography and along coastlines, *J. Geophys. Res.*, *117*, C01013, doi:10.1029/2011JC007276.

Carton, J. A., B. S. Giese, and S. A. Grodsky (2005), Sea level rise and the warming of the oceans in the Simple Ocean Data Assimilation (SODA) ocean reanalysis, *J. Geophys. Res.*, *110*, C09006, doi:10.1029/2004JC002817.

Calafat, F. M., and D. P. Chambers (2013), Quantifying recent acceleration in sea level unrelated to internal climate variability, *Geophys. Res. Lett.*, *40*, 3661–3666, doi:10.1002/grl.50731.

Calafat, F. M., D. P. Chambers, and M. N. Tsimplis (2012), Mechanisms of decadal sea level variability in the eastern North Atlantic and the Mediterranean Sea, *J. Geophys. Res.*, *117*, C09022, doi:10.1029/2012JC008285.
Calafat, F. M., D. P. Chambers, and M. N. Tsimplis (2013), Inter-annual to decadal sea-level variability in the coastal zones of the Norwegian and Siberian Seas: The role of atmospheric forcing, *J. Geophys. Res. Oceans*, *118*, 1287–1301, doi:10.1002/jgrc.20106.
Calafat, F. M., D. P. Chambers, and M. N. Tsimplis (2014), On the ability of global sea level reconstructions to determine trends and variability, *J. Geophys. Res. Oceans*, *119*, 1572–1592, doi:10.1002/2013JC009298.
Chen, X. (2014), Investigation of temperature and sea level changes in the North Sea for the period 1948–2010, PhD thesis, University of Hamburg, Hamburg, Germany.
Church, J. A., and N. J. White (2011), Sea-level rise from the late 19th to the early 21st Century, *Surv. Geophys.*, *32*(4-5), 585–602, doi:10.1007/s10712-011-9119-1.
Church, J. A., N. J. White, L. F. Konikow, C. M. Domingues, J. G. Cogley, E. Rignot, J. M. Gregory, M. R. van den Broeke, A. J. Monaghan, and I. Velcogna (2011), Revisiting the Earth's sea level and energy budgets from 1961 to 2008, *Geophys. Res. Lett.*, *38*, L18601, doi:10.1029/2011GL048794.
Church, J. A. et al. (2013), Sea level change, in *Climate Change 2013: The Physical Science Basis. Contribution of Working Group I to the Fifths Assessment Report of the Intergovernmental Panel on Climate Change*, edited by T. F. Stocker, D. Qin, and G.-K. Plattner et al., Cambridge Univ. Press, Cambridge, U. K.
Compo, G. B., et al. (2011), The twentieth century reanalysis project, *Q. J. R. Meteorol. Soc.*, *137*, 1–28, doi:10.1002/qj.776.
Dangendorf, S., T. Wahl, H. Hein, J. Jensen, S. Mai, and C. Mudersbach (2012), Mean sea level variability and influence of the North Atlantic oscillation on long-term trends in the German Bight, *Water*, *4*(1), 170–195, doi:10.3390/w4010170.
Dangendorf, S., C. Mudersbach, T. Wahl, and J. Jensen (2013a), Characteristics of intra-, inter-annual and decadal variability and the role of meteorological forcing: the long record of Cuxhaven, *Ocean Dyn.*, *63*(2–3), 209–224, doi:10.1007/s10236-013-0598-0.
Dangendorf, S., T. Wahl, E. Nilson, B. Klein, and J. Jensen (2013b), A new atmospheric proxy for sea level variability in the south-eastern North Sea: Observations and future ensemble predictions, *Clim. Dyn.*, *43*, 447–467.
Dangendorf, S., S. Müller-Navarra, J. Jensen, F. Schenk, T. Wahl, and R. Weisse (2014), North Sea storminess from a novel storm surge record since AD 1843, *J. Clim.*, *27*, 3582–3595, doi:10.1175/JCLI-D-13-00427.1.
Douglas, B. C. (1991), Global sea level rise acceleration, *J. Geophys. Res.*, *97*, 12,699–12,706.
Ducet, N., and P. Y. Le Traon (2001), A comparison of surface eddy kinetic energy and Reynolds stresses in the Guld Stream and the Kurisho current systems from merged TOPEX/Poseidon and ERS-1/2 altimetric data, *J. Geophys. Res.*, *106*, 2671–2688.
Durbin, J., and G. S. Watson (1951), Testing for serial correlation in least squares regression, II, *Biometrica*, *38*, 159–179.
Gill, A. E. (1982), *Atmosphere. Ocean Dynamics*, 662 pp., Academic, London, U. K.
Grinsted, A., J. C. Moore, and S. Jevrejeva (2004), Application of the cross wavelet transform and wavelet coherence to geophysical time series, *Nonlin. Processes Geophys.*, *11*, 561–566, doi:10.5194/npg-11-561-2004.
Haigh, I. D., R. J. Nicholls, N. C. Wells (2009), Mean sea-level trends around the English Channel over the 20th century and their wider context, *Cont. Shelf Res.*, *29*(17), 2083–2098.
Haigh, I. D., T. Wahl, R. M. Price, C. Pattiariatchi, C. M. Calafat, and S. Dangendorf (2014), Timescales for detecting a significant acceleration in sea level rise, *Nat. Commun.*, *5*, 3635.
Holgate, S. J., A. Matthews, P. L. Woodworth, L. J. Rickards, M. E. Tamisiea, E. Bradshaw, P. R. Foden, K. M. Gordon, S. Jevrejeva, and J. Pugh (2013), New data systems and products at the Permanent Servise for Mean Sea Level, *J. Coastal Res.*, *29*, 493–504, doi:10.2112/JCOASTRES-D-12-00175.1.
Ishii, M., and M. Kimoto (2009), Reevaluation of historical ocean heat content variations with varying XBT and MBT depths bias corrections, *J. Oceanogr.*, *65*, 287–299.
Jevrejeva, S., J. C. Moore, P. L. Woodworth, and A. Grinsted (2005), Influence of large scale atmospheric circulation on European sea level results based on the wavelet transform method, *Tellus, Ser. A*, *57*, 183–193, doi:10.1111/j.1600-0870.2005.00090.x.
Jevrejeva, S., J. C. Moore, P. L., A. Grinsted, A. Matthews, and G. Spada (2014), Trends and acceleration in global and regional sea level rise since 1807, *Global Planet. Change*, *113*, 11–20.
Jiang, Y., T. H. Dixon, and S. Wdowinski (2010), Accelerating uplift in the North Atlantic region as an indicator of ice loss, *Nat. Geosci.*, *3*, 404–407.
Kalnay, E., et al. (1996), The NCEP/NCAR 40-year reanalysis project, *Bull Am. Meteorol. Soc.*, *77*, 437–471. doi:10.1175/1520-0477(1996)077<0437:TNYRP>2.0.CO;2.
Kolker, S. A., and S. Hameed (2007), Meteorologically driven trends in sea level rise, *Geophys. Res. Lett.*, *34*, L23616, doi:10.1029/2007GL031814.
Krueger, O., F. Schenk, F. Feser, and R. Weisse (2013), Inconsistencies between long-term trends in storminess derived from the 20CR reanalysis and observations, *J. Clim.*, *26*, 868–874, doi:10.1175/JCLI-D-12-00309.1.
Levermann, A., A. Griesel, M. Hofmann, M. Montoya, and S. Rahmstorf (2005), Dynamic sea level changes following changes in the thermohaline circulation, *Clim. Dyn.*, *24*(4), 347–354.
Marcos, M., and M. N. Tsimplis (2007), Forcing of coastal sea level rise patterns in the North Atlantic and Mediterranean Sea, *Geophys. Res. Lett.*, *34*, L18604, doi:10.1029/2007GL030641.
Marcos, M., B. Puyol, F. M. Calafat, and G. Wöppelmann (2013), Sea level changes at Tenerife Island (NE Tropical Atlantic) since 1927, *J. Geophys. Res. Oceans*, *118*, 4899–4910, doi:10.1002/jgrc.20377.
Meehl, G. A., et al. (2007), Global climate projections, in *Climate Change 2007: The Physical Science Basis. Contribution of Working Group I to the Fourth Assessment Report of the Intergovernmental Panel on Climate Change*, edited by S. Solomon et al., pp. 433–497, Cambridge Univ. Press, Cambridge, U. K.
Mitrovica, J. X., M. E. Tamisiea, J. L. Davis, and G. A. Milne (2001), Recent mass balance of polar ice-sheets inferred from patterns of global sea-level change, *Nature*, *409*, 1026–1029, doi:10.1038/35059054.
Moore, J. C., A. Grinsted, T. Zwinger, and S. Jevrejeva (2013), Semiempirical and process-based global sea level rise projections, *Rev. Geophys.*, *51*, 484–522, doi:10.1002/rog.20015.
Orlic, M., and Z. Pasaric (2013), Semi-empirical versus process-based sea-level projections for the twenty-first century, *Nat. Clim. Change*, *3*(5), 735–738, doi:10.1038/nclimate1877.
Orvik, K. A., and Ø. Skageseth (2003), The impact of wind stress curl in the North Atlantic on the Atlantic inflow to the Nowegian Sea toward the Arctic, *Geophys. Res. Lett.*, *30*(17), 1884, doi:10.1029/2003GL017932.
Peltier, W. R. (2004), Global glacial isostacy and the surface of the Ice-Age earth: The ICE-5G(VM2) model and GRACE, *Annu. Rev. Earth Planet. Sci.*, *32*, 111–149.

Plag, H. P., and M. N. Tsimplis (1999), Temporal variability of the seasonal sea-level cycle in the North Sea and Baltic Sea in relation to climate variability, *Global Planet. Change*, *20*, 173–203.
Rahmstorf, S. (2007), A semi-empirical approach to projecting future sea-level rise, *Science*, *315*, 368–370.
Richter, K., T. Furevik, and K. A. Orvik (2009), Effect of wintertime low-pressure systems on the Atlantic inflow to the Nordic seas, *J. Geophys. Res.*, *114*, C09006, doi:10.1029/2009JC005392.
Richter, K., J. E. Ø. Nilsen, and H. Drange (2012), Contributions to sea level variability along the Norwegian coast for 1960–2010, *J. Geophys. Res.*, *117*, C05038, doi:10.1029/2011JC007826.
Riva, R. E. M., J. L. Bamber, D. A. Lavallee, and B. Wouters (2010), Sea-level fingerprint of continental water and ice mass change from GRACE, *Geophys. Res. Lett.*, *19*, L19605, doi:10.1029/2010GL044770.
Santer, B. D., T. M. L. Wigley, J. S. Boyle, D. J. Gaffen, J. J. Hnilo, D. Nychka, D. E. Parker, and K. E. Taylor (2000), Statistical significance of trends and trend differences in layer-average atmospheric temperature time series, *J. Geophys. Res.*, *105*, 7337–7356, doi:10.1029/1999JD901105.
Siegismund, F., and C. Schrum (2001), Decadal changes in the wind forcing over the North Sea, *Clim. Res.*, *18*, 39–45.
Slangen, A. B. A., C. A. Katsman, R. S. W. van de Wal, L. L. A. Vermeersen, and R. E. M. Riva (2011), Towards regional projections of twenty-first century sea-level change based on IPCC SRES scenarios, *Clim. Dyn.*, *38*, 1191–1209, doi:10.1007/s00382-011-1057-6.
Stammer, D., A. Cazenave, R. M. Ponte and M. E. Tamisiea (2013), Contemporary Regional Sea Level Changes, *Ann. Rev. in Marine Sciences*, *5*, 21–46, doi:10.1146/annurev-marine-121211-172406.
Steffen, H., and P. Wu (2011), Glacial isostatic adjustment ain Fennoscandia—A review of data and modeling, *J. Geodyn.*, *52*, 169–204.
Sturges, W., and B. C. Douglas (2011), Wind effects on estimates of sea level rise, *J. Geophys. Res.*, *116*, C06008, doi:10.1029/2010JC006492.
Tsimplis, M. N., et al. (2005), Towards a vulnerability assessment of the UK and northern European coasts: the role of regional climate variability, *Philos. Trans. R. Soc. A*, *363*, 1329–1358, doi:10.1098/rsta.2005.1571.
Vermeer, M., and S. Rahmstorf (2009), Global sea level linked to global temperature, *Proc. Natl. Acad. Sci. U. S. A.*, *106*, 21527–21532.
Von Storch, H., and F. W. Zwiers (1999), *Statistical Analysis in Climate Research*, 1st ed., Cambridge Univ. Press, Cambridge, U. K.
Von Storch, H., E. Zorita, and U. Cubasch (1993), Downscaling of global climate change estimates to regional scales: An application to Iberian rainfall in wintertime, *J. Clim.*, *6*, 1161–1171.
Wahl, T., J. Jensen, and T. Frank (2010), On analysing sea level rise in the German Bright since 1844, *Nat. Hazards Earth Syst. Sci.*, *10*, 171–179, doi:10.5194/nhess-10-171-2010.
Wahl, T., J. Jensen, T. Frank, and I. D. Haigh (2011), Improved estimates of mean sea level Changes in the German Bright over the last 166 years, *Ocean Dyn.*, *61*, 701–715, doi:10.1007/s10236-011-0383-x.
Wahl, T., I. D. Haigh, P. L. Woodworth, F. Albrecht, D. Dillingh, J. Jensen, R. Nicholls, R. Weisse, and G. Wöppelmann (2013), Observed mean sea level changes around the North Sea coastline from 1800 to present, *Earth Sci. Rev.*, *124*, 51–67.
Wakelin, S. L., P. L. Woodworth, R. A. Flather, and J. A. Williams (2003), Sea-level dependence on the NAO over the NW European Shelf, *Geophys. Res. Lett.*, *30*(7), 1403, doi:10.1029/2003GL017041.
Woodworth, P. L., F. N. Teferle, R. M. Bingley, I. Shennan, and S. D. P. Williams (2009), Trends in UK mean sea level revisited, *Geophys. J. Int.*, *176*, 19–30.
Wunsch, C., and D. Stammer (1997), Atmospheric loading and the oceanic "inverted barometer" effect, *Rev. Geophys.*, *35*, 79–107.
Yan, Z., M. N. Tsimplis, and D. Woolf (2004), Analysis of the Relationship between the North Atlantic Oscillation and sea level changes in Northwest Europe, *Int. J. Climatol.*, *24*, 743–758.
Yin, J., M. E. Schlesinger, and R. J. Stouffer (2009), Model projections of rapid sea-level rise on the northeast coast of the United States, *Nat. Geosci.*, *2*, 262–266, doi:10.1038/ngeo462.